Investigation of Transmission Properties of Plasmonic Nanostructures

By

Amimul Ihsan (132401)
S.M. Ishraq-ul-Islam (132405)
Nahian Siddique (132406)

A Thesis Submitted to the Academic Faculty in Partial Fulfillment of the Requirements for the Degree of

BACHELOR OF SCIENCE IN ELECTRICAL AND ELECTRONIC ENGINEERING

Department of Electrical and Electronic Engineering
Islamic University of Technology (IUT)
Gazipur, Bangladesh

November, 2017

Investigation of Transmission Properties of Plasmonic Nanostructures

Approved by:

Dr. Rakibul Hasan Sagor

Supervisor and Assistant Professor
Department of Electrical and Electronic Engineering,
Islamic University of Technology (IUT),
Boardbazar, Gazipur-1704

Date: 12-11-2017

CONTENTS

LIST OF FIGURES

LIST OF TABLES

ACKNOWLEDGMENTS

First and foremost, we offer our gratitude to the Almighty Allah (SWT) for bestowing us the competence to do this thesis in good health.

We are grateful to our research supervisor, Dr. Rakibul Hasan Sagor, for the support and guidance throughout our research. He created a pleasant research environment thanks to which we were able to explore many ideas without restriction. We have gained a wealth of knowledge and experience in plasmonics and research methodology through his supervision. For all of his efforts to make us better students, better researchers and most importantly better humans.

We would also like to thank Mr. Mirza Fuad Adnan for his devotion towards aiding us and our heartfelt gratitude to all the faculty members of the department of EEE, IUT for their inspiration and help.

Lastly we are thankful to our family, friends and well-wishers for their support and inspiration. Without them it would be very challenging for us to complete this goal.

ABSTRACT

Photonics managed a dynamic entry in the realm of integrated technology solving the difficulty regarding the integrated electronic devices reaching their bandwidth limitations and heat dissipation. Using light as an information carrier poses a major hurdle named as diffraction limit, which does not permit design and implementation of optical devices in the nanometer region. A feasible solution to this predicament is using materials with negative dielectric permittivity and metals below plasma frequency are proffering the opening. Amongst many plasmonic devices, ring resonators with diverse geometric configuration were investigated numerically using Finite-Difference Time-Domain scheme where design parameters were also altered to observe the effect on the transmission properties. A plasmonic directional coupler of Rat Race configuration in nanometer range was also designed and simulated to investigate the transmission efficiency and S-parameters. The results of the aforementioned structures will shed light on the credibility and novelty of the devices in pragmatic applications.

1. INTRODUCTION

Semiconductor electronic devices form the basis of todays technology and its rapid growth. It attained its ubiquity thanks to its extensive miniaturization, which enabled its impressive performance, speed and power consumption properties relative to previous technologies. However this technology is rapidly reaching its inherent limitations of speed, bandwidth and size. This is where an interesting proposition comes in. That of using light as information carriers in place of electronic signals. However the possibilities of integration and miniaturization of optical signal processing devices have thus far been quite limited and restrained. A big reason for this is the diffraction limit of electromagnetic waves. It prevents the localization of electromagnetic waves in nanoscale regions much smaller than the wavelength of the electromagnetic waves.

However this obstacle can be overcome by employing plasmonics [1]. Using plasmon-polaritons [2, 3], it is possible to localize light in regions far smaller than their wavelengths. This means that it is not only possible to design devices that are faster and consume less power, but also are smaller in size. Some possible applications of this technology include sub-wavelength imaging [4, 5], Braggs reflector [6], bio-sensing [7], meta materials [8] and also can be implemented in solar cells [9, 10].

Communications systems are already heavily dependent on optical technologies such as optical fibers which provide higher bandwidth and are more stable than electronic interconnections. The same advantage can be availed if the optical technology is used in computer chips. Also, the optical chips will not require any insulation since photons do not interact with each other, making the system lighter. However, the diffraction limit of light restricts the application of conventional optics in making nanometer scale integrated circuits. According to the diffraction limit rule, light cannot propagate through aperture that is smaller than half of its wavelength.

One of the most plasmonic devices is the ring resonator which come in diverse geometric organization with potential applications in vital sectors. Ring resonators are leading the revolution of plasmonic devices in the realm of nanotechnology.

Directional couplers, such as rate race couplers [11], are devices which are vital in microwave technology [12] for power splitting [13, 14], frequency mixing [15], phase shifting [16] and many other useful applications. The prominence of plasmonic couplers in plasmonic circuitry is paramount. Therefore, their design [17, 18, 19] and implementation have heavy impact on the barrier before the path to progress.

1.1 Overview of Surface Plasmon Polariton

Surface plasmon polaritons are electromagnetic excitations propagating at the interface between a dielectric and a conductor, evanescently confined in the perpendicular direction. These electromagnetic surface waves arise via the coupling of the electromagnetic fields to oscillations of the conductors electron plasma.

The eigenmodes of an interface between a dielectric and a metal are surface plasmon polaritons (SPPs) [20]. We refer to them as eigenmodes in the sense that they are solutions of Maxwells equations that can be formulated in the absence of an incident field. On a flat interface between dielectric and metal half-spaces with dielectric constants d and m, respectively, SPPs are transverse magnetic (TM) plane waves propagating along the interface. Assuming the interface is normal to z and the SPPs propagate along the x direction, the SPP wave vector is related to the optical frequency through the dispersion relation [21],

$$k_x = k_o\sqrt{\in_d \in_m/(\in_d + \in_m)} \tag{1.1}$$

where k_0 is the free-space wave vector. We take to be real and allow to be complex, since our main interest is in stationary monochromatic SPP fields in a finite area. The details of SPP has been discussed in chapter 2.

1.2 Literature Review

Plasmonic devices specially the plasmonic ring resonators have been a great field of interest over the recent years. Here in this section of literature review, focus have been made on the literature review of the published works on SPP propagation analysis through different structures with different geometries.

The parameters of several metals have been reported to our knowledge. Jin et al. [22] determined the modified Debye model parameters for gold which are applicable in the wavelength range of 550-950 nm. Krug et al. [23] reported the gold parameters that are applicable in the wavelength range of 700-1000 nm. W.H.P. Pernice et al. [24] extracted the parameters for Nickel using Lorentz-Drude model. A.D. Rakic et al. [25] reported the parameters for Nickel, Palladium, Titanium and 8 other metals using Lorentz-Drude and Brendel-Bormann Model. M.A. Ordal et al. [26] extracted the parameters for fourteen metals in the infrared and far-infrared range. Bends, splitters and recombination are inevitable parts of the optoelectronic devices. Several works on the analysis of SPP propagation in these shapes have been reported to our knowledge. G. Veronis et al. [27] showed that bends and splitters can be designed over a wide frequency range without much loss by keeping centre layer thickness small compared to wavelength. H. Gao et al. [28] investigated the propagation and combination of SPP in Y-shaped channels. B. Wang et al. [29] analyzed two structures which consist of splitting and recombination.

The propagation loss of SPP is very high in metal-dielectric-metal configuration of plasmonic waveguide which limits the length of propagation. Even the fabrication related disorders have far less impact on the propagation loss than the losses that occur in metallic layers of the MDM waveguide. This problem can be addressed by using both dielectric and plasmonic waveguide on the same chip. The dielectric waveguide will carry the fundamental optical mode while the plasmonic waveguide will address the sub-wavelength scale issue. This calls for the need of efficient coupling of optical modes from the dielectric waveguide to the plasmonic waveguide. Therefore, designing efficient nanoplasmonic couplers with different materials and structures can be a pioneering step in miniaturization of the integrated photonic devices. In the past years, several plasmonic couplers have been proposed by different researchers. G. Veronis et al. [30] proposed a coupler with multi-section tapers. P. Ginzburg et al. [31] reported a /4 coupler to couple optical modes from a 0.5m to 50nm wide plasmonic waveguide. D. Pile et al. [32] presented an adiabatic and a non-adiabatic tapered plasmonic coupler. R. Washleh et

al. [33] reported an analysis on nanoplasmonic air-slot coupler and its fabrication steps.

Main focus has given on designing ring resonator by placing the resonator in the core of the device [34, 35]. Emphasis was given towards pinpointing the optimum geometric configuration for the core for a wide wavelength range. The design of rat race coupler was highly motivated by the recent works of designing the coupler using Photonic Crystals [36]. The investigation was done to check the viability of nanometer scale couplers and the possible solution for their deviation from the theoretical results.

1.3 Thesis Objective

The main objective of the thesis is to accomplish novel and optimum designs of plasmonic nanostructures with pragmatic applications. In short the objectives can be described as follows:

- Implementing FDTD algorithm and dispersion parameters of materials in MATLAB.
- Designing nanometer scale plasmonic ring resonators by altering geometry of the resonator.
- Simulation of the resonators to investigate the effect of geometry on the transmission properties and identifying optimum designs.
- Designing plasmonic rat race couplers in nanometer and micrometer scale.
- Investigating the transmission properties and S-Parameters of ports of resonators by changing the radius and substrate of the coupler.

1.4 Thesis Organization

The thesis has been organized in the succeeding way:

- In chapter 2, the basic theory of SPP propagation has been described. This chapter introduces the fundamental knowledge and necessary mathematical formulations of SPP propagation at the single and double interface.
- In chapter 3, the widely used models for modeling metals have been described in detail with necessary derivations. Since SPPs are created due to the coupling of photon energy to the free electrons of metal, modeling metals is one of the key steps for the simulation of SPP propagation.
- Chapter 4 introduces the fundamentals of the FDTD algorithm for 1D and 2D simulations. We have used the ADE based general algorithm for our simulation model which is discussed in this chapter. The chapter also discusses about the absorbing boundary condition.
- Chapter 5 introduces the basic theory of ring resonators.
- In chapter 6, the design and simulation of plasmonic ring resonators by altering geometric configuration were discussed.
- In chapter 7, the geometric parameters of elliptical and rectangular ring resonators were varied to investigate their performance.
- In chapter 8, investigation of plasmonic rat race coupler designed in nanometer scale took place.

2. SPP PROPAGATIONS THEORY

2.1 Overview

Surface Plasmon Polaritons (SPP) are electromagnetic excitation that propagate in a wave like manner along a metal-dielectric medium (the dielectric could be a vacuum or air). It involves both charge motion in the metal (surface plasmon) and electromagnetic waves in the dielectric (polariton). Plasmons, which are longitudinal electron density oscillations, resemble light waves confined to the surface of a metal.

Electromagnetic wave propagation is obtained from the solution of Maxwells equation in each medium, and the associated boundary conditions. Maxwells equations of macroscopic electromagnetism are presented below.

From Gauss Law for the electric field

$$\nabla.D = \rho_{ext} \tag{2.1}$$

From Gausss Law for the magnetic field

$$\nabla.B = 0 \tag{2.2}$$

From Faradays Law

$$\nabla \times E = -\frac{\partial B}{\partial t} \tag{2.3}$$

From Amperes Law

$$\nabla \times H = J_{ext} + \frac{\partial D}{\partial t} \tag{2.4}$$

Here,

E is the electric field vector in volt per meter

D is the electric flux density vector in coulombs per square meter

H is the magnetic field vector in amperes per meter

B is the magnetic flux density vector in webbers per square meter

ρ_{ext} is the charge density

J_{ext} is the current density

The four macroscopic fields can be also linked further via the polarization P and magnetization M by

$$D = \varepsilon_o E + P \tag{2.5}$$

$$H = \frac{1}{\mu_o} B - M \tag{2.6}$$

Now this equations can be simplified for linear, isotropic, nonmagnetic media as

$$D = \varepsilon_o \varepsilon_r E \tag{2.7}$$

$$B = \mu_o \mu_r H \tag{2.8}$$

where,

ε_0 is the electric permittivity of vacuum in Farad per meter.

μ_0 is the magnetic permeability of vacuum in Henry per meter.

ε_r is the relative permittivity.

μ_0 is the relative permeability.

2.2 The Electromagnetic Wave Equation

The EM wave equation which describes the field amplitude in time and space can be derived from Maxwells equations. The wave equation can be derived

by taking curl of Faradays law

$$\nabla \times \nabla \times E = -\frac{\partial B}{\partial t} \tag{2.9}$$

or,

$$\nabla \times \nabla \times E = \nabla \times (-\mu \frac{\partial H}{\partial t}) \tag{2.10}$$

With the identities $\nabla \times \nabla \times E = \nabla(\nabla.E) - \nabla^2 E$ and $\nabla \times H = \varepsilon \frac{\partial E}{\partial t}$ we can simplify the above equation as

$$\nabla(\nabla.E) - \nabla^2 E = -\mu\varepsilon \frac{\partial^2 y}{\partial t^2} \tag{2.11}$$

From Gausss law we can conclude that the divergence of E in a constant permittivity over space is zero, i.e. $\nabla.E = 0$

Therefore, the final wave equation for electric field will be

$$\nabla^2 E - \mu\varepsilon \frac{\partial^2 E}{\partial t^2} = 0 \tag{2.12}$$

Similarly the wave equation for magnetic field can be derived as

$$\nabla^2 H - \mu\varepsilon \frac{\partial^2 H}{\partial t^2} = 0 \tag{2.13}$$

So, the general form of wave equation can be written as

$$\nabla^2 E - \frac{\varepsilon}{C^2} \frac{\partial^2 E}{\partial t^2} = 0 \tag{2.14}$$

Where $c = \frac{1}{\sqrt{\varepsilon_0 \mu_0}}$ = velocity of light

The solution of wave equation is a harmonic function in time and space. Now if we assume this as a harmonic time dependence of the electric field,

$$E(r,t) = E(r)e^{-j\omega t} \tag{2.15}$$

Therefore we get the Helmholtz equation

$$\nabla^2 E + K_0^2 \varepsilon E = 0 \tag{2.16}$$

where the vector of propagation $K_0 = \frac{\omega}{c}$ in free space.

For simplicity let us assume the propagation of wave is along the x-direction of the Cartesian co-ordinate system and no spatial variation in y-direction. So we can write

$$E(x, y, z) = E(z)e^{j\beta z} \tag{2.17}$$

where $\beta = K_x$ which is called the propagation constant.

Now inserting the value of E the wave equation will be

$$\frac{\partial^2 E(z)}{\partial z^2} + (K_0^2\varepsilon - \beta^2)E = 0 \tag{2.18}$$

Similarly we can derive the equation for the magnetic field H. The field E and H can be decomposed in cartesian co-ordinate system as

$$E = E_x \overrightarrow{a}_x + E_y \overrightarrow{a}_y + E_z \overrightarrow{a}_z \tag{2.19}$$

$$H = H_x \overrightarrow{a}_x + H_y \overrightarrow{a}_y + H_z \overrightarrow{a}_z \tag{2.20}$$

For Harmonic time dependence $\frac{\partial}{\partial t} = -j\omega$ and by solving the Amperes law and Faradays law, we get

$$\frac{\partial E_z}{\partial y} - \frac{\partial E_y}{\partial z} = j\omega\mu_0 H_x \tag{2.21}$$

$$\frac{\partial E_x}{\partial z} - \frac{\partial E_z}{\partial x} = j\omega\mu_0 H_y \tag{2.22}$$

$$\frac{\partial E_y}{\partial x} - \frac{\partial E_x}{\partial y} = j\omega\mu_0 H_z \tag{2.23}$$

$$\frac{\partial H_z}{\partial y} - \frac{\partial H_y}{\partial z} = j\omega\varepsilon_0\varepsilon E_x \tag{2.24}$$

$$\frac{\partial H_x}{\partial z} - \frac{\partial H_z}{\partial x} = j\omega\varepsilon_0\varepsilon E_y \tag{2.25}$$

$$\frac{\partial H_y}{\partial x} - \frac{\partial H_x}{\partial y} = j\omega\varepsilon_0\varepsilon E_z \tag{2.26}$$

As the propagation is in x-direction in the form of $e^{j\beta x}$ which follows $\frac{\partial}{\partial \beta} = -j\beta$. The homogeneity in y-direction makes /x=0. So the equation will be simplified as

$$-\frac{\partial E_y}{\partial z} = j\omega\mu_0 H_x \tag{2.27}$$

$$\frac{\partial E_x}{\partial z} - j\beta E_z = j\omega\mu_0 H_y \tag{2.28}$$

$$j\beta E_y = j\omega\mu_0 H_z \tag{2.29}$$

$$\frac{\partial H_y}{\partial z} = j\omega\varepsilon_0\varepsilon E_x \tag{2.30}$$

$$\frac{\partial H_x}{\partial z} - j\beta H_z = j\omega\varepsilon_0\varepsilon E_y \tag{2.31}$$

$$j\beta H_y = j\omega\varepsilon_0\varepsilon E_z \tag{2.32}$$

The solution of the above equation can be characterized by two sets of solution with the polarized characteristics which are, Transverse Magnetic (TM) modes and Transverse Electric (TE) modes. The equations belonging to TM modes are

$$E_x = -j\frac{1}{\omega\varepsilon_0\varepsilon}\frac{\partial H_y}{\partial z} \tag{2.33}$$

$$E_z = -\beta\frac{1}{\omega\varepsilon_0\varepsilon}H_y \tag{2.34}$$

Therefore, the wave equation for TM Polarized wave will be

$$\frac{\partial^2 H_y}{\partial z^2} + (K_0^2\varepsilon - \beta^2)H_y = 0 \tag{2.35}$$

Similarly the TE polarized equations are will be

$$H_x = j\frac{1}{\omega\mu_0}\frac{\partial E_y}{\partial z} \tag{2.36}$$

$$H_y = \beta\frac{1}{\omega\mu_0}E_y \tag{2.37}$$

And the corresponding TE wave equation will be

$$\frac{\partial^2 E_y}{\partial z^2} + (K_0^2\varepsilon - \beta^2)E_y = 0 \tag{2.38}$$

2.3 SPP at Single Interface

The simplest configuration for SPP propagation is at a single interface. This is between a dielectric of dielectric constant ε_2 and a metal of negative dielectric constant ε_1. For the metal, the bulk plasmon frequency will be ω_p and the amplitude decays perpendicular to the z-direction. For the TM solutions in both spaces: metal and dielectric will be for z¿0

$$H_z(z) = A_2 e^{j\beta x} e^{-k_2 z} \tag{2.39}$$

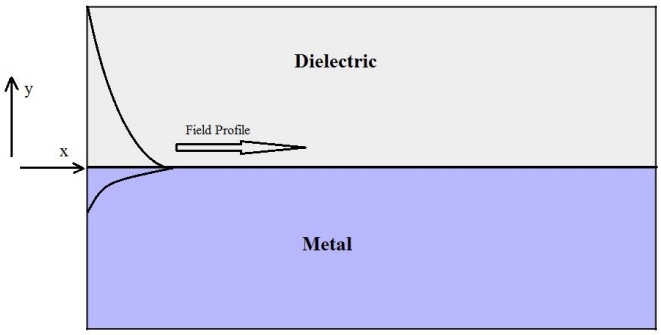

Fig. 2.1: SPP at the single interface

$$E_x(z) = jA_2 \frac{1}{\omega\varepsilon_0\varepsilon_2} k_2 e^{j\beta x} e^{-k_2 z} \tag{2.40}$$

$$E_z(z) = -A_1 \frac{\beta}{\omega\varepsilon_0\varepsilon_2} e^{j\beta x} e^{-k_2 z} \tag{2.41}$$

and for z <0

$$H_y(z) = A_1 e^{j\beta x} e^{k_1 z} \tag{2.42}$$

$$E_x(z) = -jA_1 \frac{1}{\omega\varepsilon_0\varepsilon_1} k_1 e^{j\beta x} e^{k_1 z} \tag{2.43}$$

$$E_x(z) = -A_1 \frac{\beta}{\omega\varepsilon_0\varepsilon_1} e^{j\beta x} e^{-k_1 z} \tag{2.44}$$

The continuity of H_y and $\varepsilon_i E_z$ at the metal dielectric gives $A_1 = A_2$ and

$$\frac{k_2}{k_1} = -\frac{\varepsilon_2}{\varepsilon_1} \tag{2.45}$$

The surface wave exists at the metal dielectric interface with opposite sign of their real dielectric permittivities. So, we can write

$$k_1^2\varepsilon = \beta^2 - k_0^2\varepsilon_1 \tag{2.46}$$

$$k_2^2\varepsilon = \beta^2 - k_0^2\varepsilon_2 \tag{2.47}$$

The dispersion relation of SPPs propagation can be found as

$$\beta = k_0 \sqrt{\frac{\varepsilon_1\varepsilon_2}{\varepsilon_1 + \varepsilon_2}} \tag{2.48}$$

The TE surface modes can be expressed as

$$E_y(z) = A_2 e^{j\beta x} e^{-k_2 z} \tag{2.49}$$

$$H_x(z) = -jA_2\frac{\beta}{\omega\mu_0}k_2e^{j\beta x}e^{-k_2z} \tag{2.50}$$

$$H_z(z) = -A_2\frac{\beta}{\omega\mu_0}k_2e^{j\beta x}e^{-k_2z} \tag{2.51}$$

For $z > 0$, and

$$E_y(z) = A_1e^{j\beta x}e^{-k_1z} \tag{2.52}$$

$$H_x(z) = jA_1\frac{\beta}{\omega\varepsilon_0\varepsilon_1}k_1e^{j\beta x}e^{k_1z} \tag{2.53}$$

$$H_z(z) = A_1\frac{\beta}{\omega\varepsilon_0\varepsilon_1}k_2e^{j\beta x}e^{k_1z} \tag{2.54}$$

For $z < 0$, the continuity of E_y and H_y requires

$$A_1(k_1 + k_2) = 0 \tag{2.55}$$

The surface requires that the real part of k1 and k2 should be greater than zero for confinement. This will be satisfied if $A_1 = A_2 = 0$. Therefore no surface modes for the TE polarization. SPP only exist for TM mode polarization.

2.4 SPP at Double Interface

The two most prominent double interface configurations of SPP waveguides are the Metal-Dielectric-Metal (MDM) and Dielectric-Metal-Dielectric (DMD). In these cases SPPs are formed on both interfaces. When the distance is shorted than decay distance, it forms coupled mode of SPP. This coupled mode of propagation can be also be sub-divided into even and odd modes, as shown in the figure.

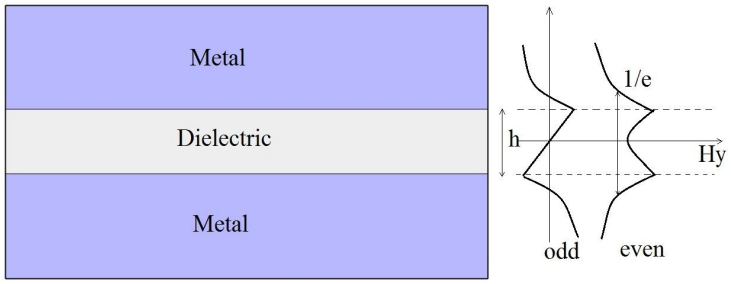

Fig. 2.2: SPP at the double interface

3. MATERIAL MODELLING WITHIN OPTICAL RANGE

3.1 Overview

At low frequencies or for long wavelengths metals act as perfect conductors. Since it has zero field, they do not show any dispersive behavior. But at higher frequencies as those found in the optical range, metals behave as dispersive materials which implies that there exists field inside metal. And in frequencies higher than the optical range, metals act as dielectrics. Thus, properties of SPPs depend highly on the material response to light.

Three vectors can determine the behavior of any material in the presence of an external oscillation electromagnetic field, three vectors can determine the behavior of any material. These are

D-Electric flux density E-Electric field intensity P-Polarization density

The corresponding equations in the frequency domain are

$$D(\omega) = \varepsilon(\omega)E(\omega) \tag{3.1}$$

$$P(\omega) = \varepsilon_0\chi(\omega)E(\omega) \tag{3.2}$$

$$D(\omega) = \varepsilon_0 E(\omega) + P(\omega) \tag{3.3}$$

Combining these two equations we get

$$D(\omega) = \varepsilon_0 E(\omega)(1 + \chi(\omega)) \tag{3.4}$$

Where χ is the electric susceptibility which measures how easily it is polarized in response to an applied electric field, and it is a dimensionless quantity.

Finally the relation between the permittivity and susceptibility is

$$\varepsilon(\omega) = \varepsilon_0(1 + \chi(\omega)) \tag{3.5}$$

So the relative permittivity will be

$$\varepsilon_r(\omega) = 1 + \chi(\omega) \tag{3.6}$$

For linear isotropic materials (for e.g. glass) this value becomes simple. But for a dispersive material, the frequency dependent permittivity and susceptibility needs to be modeled precisely for predicting the response of the material for a given electromagnetic excitation. Some widely used material models are Drude model, Lorentz model, and Debye model.

3.2 Different Material Models

3.2.1 The Drude Model

The Drude model of electrical conduction was first developed by Paul Drude. In the model he described the metal as a volume filled with stationary positive ions, immersed in a gas of electrons following the kinetic theory of gases. These electrons are free to move inside the metal without any interaction with each other. The electrons in a metal are subjected to two forces, such as

1.Driving force F_d 2.Damping force F_g

The driving force and the damping force can be expressed as

$$F_d = qE = -eE \tag{3.7}$$

$$F_g = -\Gamma\nu \tag{3.8}$$

As the two forces are opposite to each other, the resultant force will be

$$F = F_d - F_g \tag{3.9}$$

From Newtons first law of motion we can write

$$mr" = -eE + \Gamma r' \tag{3.10}$$

where, m is the mass of an electron Γ is the damping constant in Newton second per meter r is the displacement in meter v is the velocity of the electron q is the electron's charge The prime indicates differentiation order with respect to time.

For time harmonic electric field and time harmonic displacement the equation will be

$$E(t) = E_0 e^{-j\omega t} \Leftrightarrow E(\omega) \tag{3.11}$$

$$r(t) = R_0 e^{-j\omega t} \Leftrightarrow R(\omega) \tag{3.12}$$

From equaion 3.10 the frequency domain form will be

$$mR"(\omega) - \Gamma m R'(\omega) + eE(\omega) = 0 \tag{3.13}$$

The derivatives of frequency domain will give

$$-m\omega^2 R"(\omega) + j\omega\Gamma m R'(\omega) + eE(\omega) = 0 \tag{3.14}$$

Simplifying the above equation, the displacement R will give

$$R(\omega) = \frac{-e}{m(j\Gamma\omega - \omega^2)} E(\omega) \tag{3.15}$$

The polarization for n number of electrons will be

$$P(\omega) = -neR(\omega) \tag{3.16}$$

or,

$$P(\omega) = \frac{e^2 n}{m(j\Gamma\omega - \omega^2)} E(\omega) \tag{3.17}$$

An expression for the susceptibility can also be obtained from the above equation and that will be

$$\frac{P(\omega)}{\varepsilon_0 E(\omega)} = \frac{e^2 n}{\varepsilon_0 m(j\Gamma\omega - \omega^2)} = \chi(\omega) \tag{3.18}$$

Now substituting this value in equation 3.6 we get

$$\varepsilon_r(\omega) = 1 + \frac{e^2 n}{\varepsilon_0 m(j\Gamma\omega - \omega^2)} \tag{3.19}$$

If we consider $_p$ as the plasma frequency that will provide

$$\omega_p^2 = \frac{e^2 n}{\varepsilon_0 m} \tag{3.20}$$

So, the frequency dependent flux density will be

$$D(\omega) = \varepsilon_0 (1 + \frac{\omega_p^2}{(j\Gamma\omega - \omega^2)}) E(\omega) \tag{3.21}$$

For low frequency, the term $\Gamma\omega << 1$ therefore, the dispersive relation can be reduced to

$$D(\omega) = \varepsilon_0 (1 - \frac{\omega_p^2}{\omega^2}) E(\omega) \tag{3.22}$$

3.2.2 The Lorentz Model

The Lorentz models gives a simpler picture of the atom. This models is helpful in visualizing atom-field interactions. Lorentz modeled and atom as a mass (nucleus) connected to another smaller mass (electron). However, electrons in the Lorentz models do not move freely inside the metal but are instead bound to atoms. Thus there exists a restoring force between them. This may be denoted by F_r.

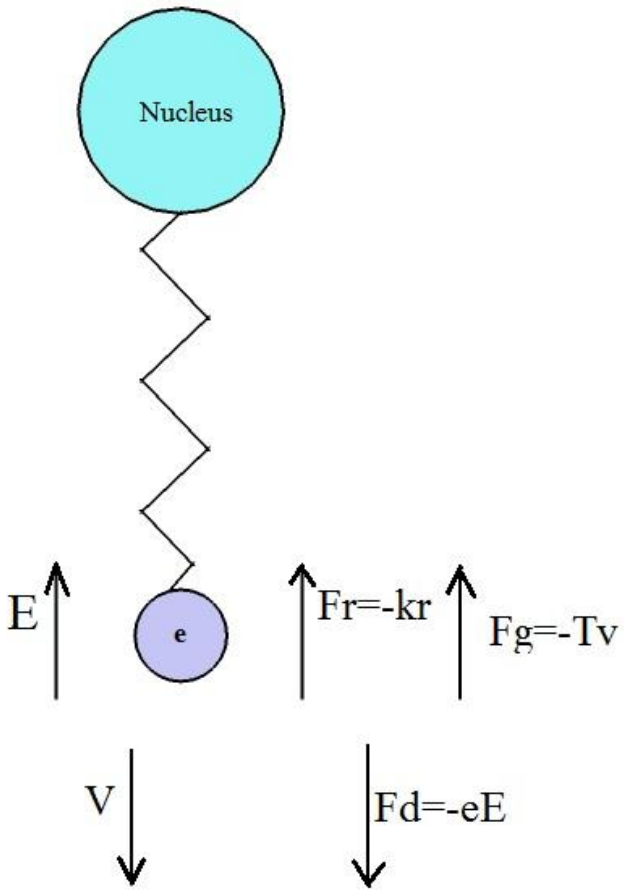

Fig. 3.1: Lorentz Model

The restoring force can be written as

$$F_r = -kr \tag{3.23}$$

where k is the spring constant in Newtons per meter.

Similarly from the law of motion we can say that,

$$mr" + \Gamma mr'(\omega) + mkr + eE = 0 \tag{3.24}$$

In frequency domain the above equation will be

$$R(\omega)(m\omega_0^2 + j\omega\Gamma m - m\omega^2 - eE(\omega)) = 0 \tag{3.25}$$

Considering the natural frequency $\omega_0 = \sqrt{\frac{k}{m}}$ we get

$$R(\omega) = \frac{-e}{m(\omega_0^2 + j\omega\Gamma - \omega^2)}E(\omega) \tag{3.26}$$

Therefore the susceptibility can be found as

$$\frac{P(\omega)}{\varepsilon_0 E(\omega)} = \frac{e^2 n}{\varepsilon_0 m(\omega_0^2 + j\omega\Gamma - \omega^2)} = \chi(\omega) \tag{3.27}$$

So from the equation 3.4 the expression for D can be expressed in frequency domain as

$$D(\omega) = \varepsilon_0(1 + frac\omega_p^2\omega_0^2 + j\omega\Gamma - \omega^2) \tag{3.28}$$

3.2.3 The Lorentz-Drude Model

In the Lorentz-Drude (LD) model, electrons in two states oscillate inside the metal and they contribute to the permittivity. The free electrons contribute a permittivity of the Drude model, and the bound electrons contribute a permittivity of the Lorentz model. The permittivity in the LD model is given by

$$\varepsilon = \varepsilon_{free} + \varepsilon_{bound} \tag{3.29}$$

where,

$$\varepsilon_{free} = 1 + \frac{\omega_p}{(j\Gamma\omega - \omega^2)} \tag{3.30}$$

$$\varepsilon_{bound} = \frac{\omega_p}{\omega_0 + j\Gamma\omega - \omega^2} \tag{3.31}$$

Therefore combining both the models together the electric field density D in frequency domain will be

$$D(\omega) = \varepsilon_0(1 + \frac{\omega_p}{j\Gamma\omega - \omega^2} + \frac{\omega_p}{\omega_0 + j\Gamma\omega - \omega^2})E(\omega) \tag{3.32}$$

3.2.4 The Debye Model

The Debye model was first developed by Peter Debye in the year 1912. According to the Debye model, materials are made of electric dipoles so that when an electric field is applied, these dipoles follow the behavior of the applied field with some relaxation time. If the electric field is oscillating at a slow frequency, then the polarization will be strong. On the other hand, a fast oscillating field means low polarization. From another point of view, materials with long relaxation times have low polarization or no polarization at all, and materials with short relaxation times have strong polarization.

Metals are known to have very short relaxation times. Thus, polarization in metals is strong. If a DC electric field is applied to a dielectric, the polarization takes some time to follow the electric field. At steady state, it will be

$$P(t) = P_{\infty}(1 - e^{-t/\tau}) \tag{3.33}$$

where *P(t)* is the instantaneous polarization P_{∞} is the polarization in the steady state is the time constant. The derivative of the above equation will be

$$\frac{dP(t)}{dt} = \frac{1}{\tau} P_{\infty} e^{-t/\tau} \tag{3.34}$$

Now combining both the equations we get

$$P(t) = P_{\infty} - \tau \frac{dP(t)}{dt} \tag{3.35}$$

As $P_{\infty} = \varepsilon_0(\varepsilon - 1)E(t)$, the equation will be reduced to

$$P(t) = \varepsilon_0(\varepsilon - 1)E(t) - \tau \frac{dP(t)}{dt} \tag{3.36}$$

or,

$$\varepsilon_0(\varepsilon - 1)E(t) = P(t) + \tau \frac{dP(t)}{dt} \tag{3.37}$$

In the frequency domain the equation will be

$$\varepsilon_0(\varepsilon - 1)E(\omega) = P(\varepsilon) + j\omega\tau P(\omega) \tag{3.38}$$

or,

$$P(\omega) = \frac{\varepsilon_0(\varepsilon - 1)}{1 + j\omega\tau} E(\omega) \tag{3.39}$$

The susceptibility can be expressed as

$$\frac{\varepsilon - 1}{1 + j\omega\tau} = \frac{P(\omega)}{\varepsilon_0 E(\omega)} = \chi(\omega) \tag{3.40}$$

And the relative permittivity will be

$$\varepsilon_0(\omega) = \frac{\varepsilon - 1}{1 + j\omega\tau} + 1 = 1 + \chi(\omega) \tag{3.41}$$

For the permittivity function to fit in the range from 0 frequency to infinite frequency, the boundary conditions are $\varepsilon_r(0) = \varepsilon_s(0)$ and $\varepsilon_r(\infty) = \varepsilon_\infty(0)$ So,

$$\varepsilon(\omega) = \varepsilon_\infty + \frac{(\varepsilon_s - \varepsilon_\infty)}{1 + j\omega\tau} \tag{3.42}$$

To take into account the material losses that SPPs encounter, another term is added with the permittivity of metal. So the above equation can be expanded to

$$\varepsilon(\omega) = \varepsilon_\infty + \frac{(\varepsilon_s - \varepsilon_\infty)}{1 + j\omega\tau} - j\frac{\sigma}{\omega\varepsilon_0} \tag{3.43}$$

where

$$\varepsilon'(\omega) = \varepsilon_\infty + \frac{(\varepsilon_s - \varepsilon_\infty)\omega\tau}{1 + j\omega^2\tau^2} \tag{3.44}$$

$$\varepsilon"(\omega) = \varepsilon_\infty + \frac{(\varepsilon_s - \varepsilon_\infty)\omega\tau}{1 + j\omega^2\tau^2} + \frac{\sigma}{\omega\varepsilon_0} \tag{3.45}$$

3.3 Material Dispersion

Dispersion can be defined as the variation of the propagation waves wavelength with frequency. It is also sometimes defined as the variation of propagating waves wave number $k = \frac{2\pi}{\lambda}$ with angular frequency $\omega = 2\pi f$. So the one dimensional wave equation will be

$$\frac{\partial^2 u}{\partial t^2} = \upsilon^2 \frac{\partial^2 u}{\partial x^2} \tag{3.46}$$

where

$$\upsilon^2 = \frac{1}{\varepsilon\mu} \tag{3.47}$$

The solution of the above wave equation can be written in phasor form as

$$u(x,t) = e^{j(\omega t - kx)} \tag{3.48}$$

Now putting this value in the wave equation we get

$$(j\omega)^2 e^{j(\omega t - kx)} = \upsilon^2 (-jk)^2 e^{j(\omega t - kx)} \tag{3.49}$$

Finally from this equation we greater

$$k = \pm \frac{\omega}{v} \tag{3.50}$$

The + sign is for $-x$ directed wave propagation and $-$ sign is for $+x$ directed wave propagation. The magnetic flux density and electric flux density for dispersive medium are

$$D(\omega) = \varepsilon(\omega) E \tag{3.51}$$

$$B(\omega) = \mu(\omega) H \tag{3.52}$$

Here both $\varepsilon(\omega)$ and $\mu(\omega)$ are freque dependent functions.

4. OVERVIEW OF FINITE-DIFFERENCE TIME DOMAIN METHOD

4.1 The Yee Algoritm

The algorithm used in FDTD simulations is known as the Yee algorithm. The original proposal was intended for homogeneous, isotropic and lossless media based on discretizing the volume into cells in Cartesian coordinates. The Yee algorithm solves for both electric and magnetic fields using the coupled Maxwells time-dependent curl equations, rather than solving for the electric field alone (or the magnetic field alone) with a wave equation.

The method begins with two of Maxwells equations:

$$D\frac{\partial \overrightarrow{H}}{\partial t} = -\frac{1}{\mu}\nabla \times \overrightarrow{E} \tag{4.1}$$

$$D\frac{\partial \overrightarrow{E}}{\partial t} = \frac{1}{\varepsilon}\nabla \times \overrightarrow{H} \tag{4.2}$$

The electric and magnetic fields are three dimensional vectors. Each equation can be converted into three coupled scalar first order differential equations. The derivatives are both in space and time. The curl operations of equations 4.1 and equation 4.2 yields the following six equations in Cartesian coordinates

$$\frac{\partial E_z}{\partial y} - \frac{\partial E_y}{\partial z} = \mu\frac{\partial H_x}{\partial t} \tag{4.3}$$

$$\frac{\partial E_x}{\partial z} - \frac{\partial E_z}{\partial x} = \mu\frac{\partial H_y}{\partial t} \tag{4.4}$$

$$\frac{\partial E_y}{\partial x} - \frac{\partial E_x}{\partial y} = \mu\frac{\partial H_z}{\partial t} \tag{4.5}$$

$$\frac{\partial H_z}{\partial y} - \frac{\partial H_y}{\partial z} = \varepsilon \frac{\partial E_x}{\partial t} \tag{4.6}$$

$$\frac{\partial H_x}{\partial z} - \frac{\partial H_z}{\partial x} = \varepsilon \frac{\partial E_y}{\partial t} \tag{4.7}$$

$$\frac{\partial H_y}{\partial x} - \frac{\partial H_x}{\partial y} = \varepsilon \frac{\partial E_z}{\partial t} \tag{4.8}$$

Then the scalar differential equations are converted into difference equations. In order to do that, discretization is required for both space and time. For space discretization, Yee visualized the field components arranged within a unit cell (voxel). The electric field components are stored on the corresponding cell edges, while the magnetic field components are stored on the corresponding face centers. The fields are located in a way where each E component is surrounded by four H components and vice versa, which leads to a spatially coupled system of field circulations corresponding to the law of Faraday and Ampere. The figure 4.1 shows the Yees spatial grid.

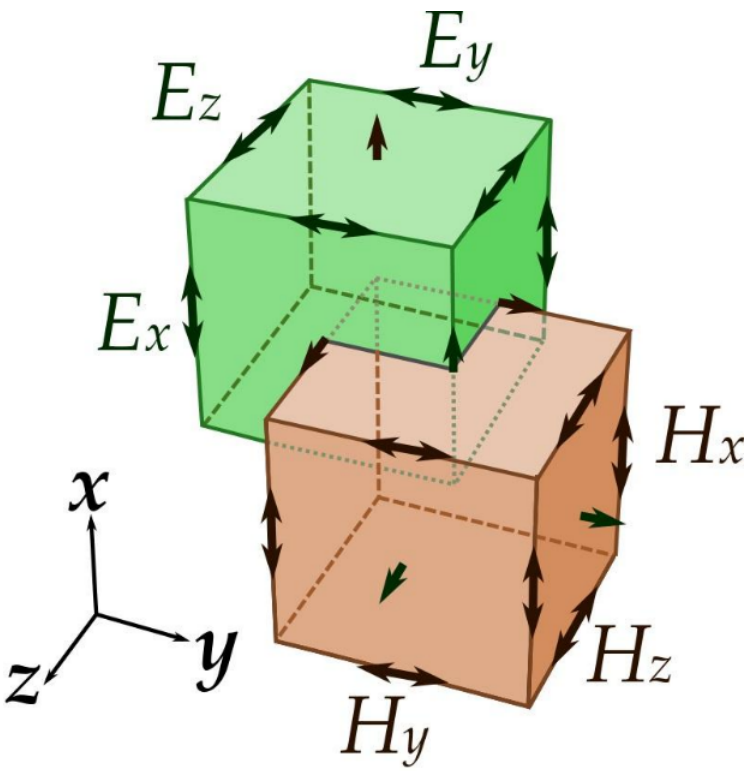

Fig. 4.1: Yee's Spatial Grid

Considering a two dimensional TM (Transverse Magnetic) polarized field

case,

$$\frac{\partial E_x}{\partial t} = \frac{1}{\varepsilon}\frac{\partial H_z}{\partial y} \tag{4.9}$$

$$\frac{\partial E_y}{\partial t} = \frac{1}{\varepsilon}\frac{\partial H_z}{\partial x} \tag{4.10}$$

$$\frac{\partial H_z}{\partial x} = \frac{1}{\mu}(\frac{\partial E_x}{\partial y} - \frac{\partial E_y}{\partial x}) \tag{4.11}$$

Central difference approximation is applied in each of the equations 4.9, 4.10 and 4.11 which finally conclude in a spatial scalar difference equations in 4.12, 4.13 and 4.14.

$$\frac{\partial E_x}{\partial t} = \frac{1}{\varepsilon}\frac{H_z(i,j) - H_z(i,j-1)}{\Delta y} \tag{4.12}$$

$$\frac{\partial E_y}{\partial t} = \frac{1}{\varepsilon}\frac{H_z(i,j) - H_z(i-1,j)}{\Delta x} \tag{4.13}$$

$$\frac{\partial H_z}{\partial t} = \frac{1}{\mu}(\frac{E_x(i,j+1) - E_x(i,j)}{\Delta y} - \frac{E_y(i+1,j) - E_y(i-1,j)}{\Delta x}) \tag{4.14}$$

In order to consider the time derivatives, the time axis is to be considered as shown in the figure. The Electric and Magnetic field are mapped half a step apart along the time axis. Again applying the central difference approximation the equations 4.12, 4.13 and 4.14 become:

$$\frac{E_x^{n+1}(i,j+\frac{1}{2}) - E_x^n(i+\frac{1}{2},j)}{\Delta t} = \frac{1}{\varepsilon}\frac{H_z^{n+\frac{1}{2}}(i+\frac{1}{2},j) - H_z^{n+\frac{1}{2}}(i+\frac{1}{2},j-\frac{1}{2})}{\Delta y} \tag{4.15}$$

$$\frac{E_y^{n+1}(i,j+\frac{1}{2}) - E_y^n(i,j+\frac{1}{2})}{\Delta t} = -\frac{1}{\varepsilon}\frac{H_z^{n+\frac{1}{2}}(i+\frac{1}{2},j+\frac{1}{2}) - H_z^{n+\frac{1}{2}}(i-\frac{1}{2},j+\frac{1}{2})}{\Delta y} \tag{4.16}$$

$$\frac{H_z^{n+\frac{1}{2}}(i+\frac{1}{2},j+\frac{1}{2}) - H_z^{n-\frac{1}{2}}(i+\frac{1}{2},j+\frac{1}{2})}{\Delta t} = -\frac{1}{\mu}\left(\frac{E_x^{n+1}(i+\frac{1}{2},j+1) - E_x^n(i+\frac{1}{2},j)}{\Delta y} - \frac{E_y^n(i+1,j+\frac{1}{2}) - E_y^n(i,j+\frac{1}{2})}{\Delta x}\right) \tag{4.17}$$

Each field component depends on the field of previous time step itself and the surrounding component in Yees algorithm.

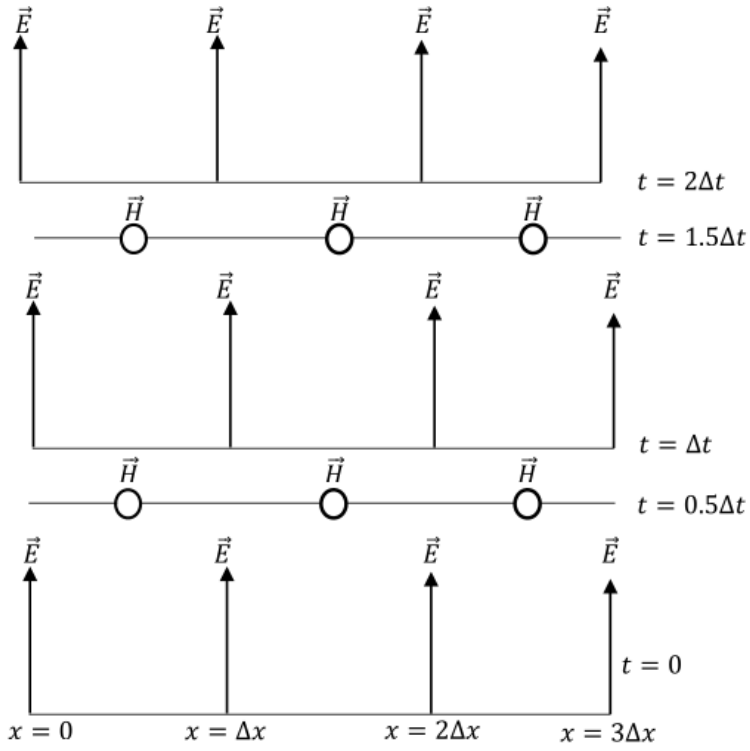

Fig. 4.2: The temporal scheme of FDTD method

Numerical stability of the Yee algorithm is required to be ensured. In an unstable algorithm the computed magnitude of electric and magnetic field components will gradually increase without limit with the progression of simulation. To guarantee numerical stability, the EM fields propagation should not be faster than the al-lowed limit which is imposed by the phase velocity within the material. This is done by limiting time step t using the Courant-Friedrichs-Lewy criterion for the general Yee FDTD grid as follows:

$$\Delta t \leq \left\{ \frac{1}{v\sqrt[p]{\frac{1}{(\Delta x)^2} + \frac{1}{(\Delta y)^2} + \frac{1}{(\Delta z)^2}}} \right\} \tag{4.18}$$

where Δx, Δy and Δz indicate the spatial Cartesian grid increments.

4.2 Absorbing Boundary conditions (ABC)

In FDTD method, a space of theoretically infinite extent with a finite computational cell is simulated due to limited computer resources. The boundary is said to be ideally absorbing, without any non-physical reflection back to the region. To accomplish this, a number of boundary conditions such as Berengers perfectly matched layer (PML), have been proposed. An artificial layer surrounds the computational domain so that most of the outgoing waves are absorbed. The electromagnetic fields are made to attenuate rapidly until they become equal to zero, so that they do not produce any reflections.

4.3 Material Dispersion in FDTD

The material is said to be dispersive when the permittivity and permeability of a material are functions of frequency. In reality the assumption of constant relative permittivity is not absolutely correct. Because by doing so, instantaneous polarization of charge within a material is being assumed. In order to exploit the realistic wave propagation, dispersive FDTD techniques become necessary. The existing FDTD based algorithms for the analysis of material dispersion can be categorized into three types:

1. The auxiliary differential equation (ADE)
2. The Z-transform methods and
3. Methods base on discrete convolution of the dispersion relation or the recursive convolution (RC) method

We will highlight on the ADE dispersive FDTD method as we have applied in material modeling. The other methods will also be briefly discussed.

4.3.1 The Auxiliary Differential Equation (ADE)

Taflove introduced the auxiliary differential equation to the FDTD modeling in order to integrate the dispersion relation into the model. The dispersion relation is converted from frequency domain to time domain through Fourier

transform in the basic step of the procedure. The Fourier transform results in a relationship between the new E field value and the previous E and D values, which can be added to the algorithm to update the E fields. The new algorithm with ADE becomes

$$\frac{\partial}{\partial t}H_z = -\frac{1}{\mu}(\frac{\partial E_x}{\partial y} - \frac{\partial E_y}{\partial x}) \tag{4.19}$$

$$\frac{\partial}{\partial t}D_x = \frac{\partial H_z}{\partial y} \tag{4.20}$$

In order to get the function relating D to E in a dispersive medium, we start with

$$D(\omega) = \varepsilon_0 \frac{\sigma}{j\omega} E(\omega) \tag{4.21}$$

Multiplying by $j\omega$

$$j\omega D(\omega) = \varepsilon_0 \sigma E(\omega) \tag{4.22}$$

Applying the Fourier transform in equation 4.22

$$\frac{d}{dt}D(t) = \varepsilon_0 \sigma E(t) \tag{4.23}$$

Discretizing equation 4.20 equation using forward difference method

$$\frac{D^n - D^{n-1}}{\Delta t} = \varepsilon_0 \sigma E(t) \tag{4.24}$$

Finally solving for E, we find the update equation

$$E^n = \frac{D^n - D^{n-1}}{\varepsilon_0 \sigma \Delta t} \tag{4.25}$$

4.3.2 The Z-transform Methods

The Z-transform is a faster method compared to ADE method. Sullivan used the Z-transform method for the first time in order to introduce the dispersion relation into the FDTD algorithm.

The Z-transform of the equation

$$D(\omega) = \varepsilon(\omega) E(\omega) \tag{4.26}$$

is

$$D(z) = \varepsilon(z) \Delta t E(z) \tag{4.27}$$

where $\varepsilon(z)$ is the z-transform of $\varepsilon(\omega)$ and is the sampling period. As already done in ODE, let us consider the material dispersion as $\frac{\sigma}{j\omega}$, the relation between D and E is given by

$$D(\omega) = \frac{\sigma\varepsilon_0}{1 - z^{-1}}\Delta t E(z) \tag{4.28}$$

Multiplying by $(1 - z^{-1})$, we find

$$D(z)(1 - z^{-1}) = \sigma\varepsilon_0 E(z) \tag{4.29}$$

or,

$$D(z) - z^{-1}D(z) = \sigma\varepsilon_0 E(z) \tag{4.30}$$

performing inverse z-transform

$$D^n - D^{n-1} = \sigma\varepsilon_0\Delta t E^n \tag{4.31}$$

Finally, for solving E from equation 4.28, we find

$$E^n = \frac{D^n - D^{n-1}}{\sigma\varepsilon_0\Delta t} \tag{4.32}$$

Which is same as the final update equation derived by ADE method.

4.3.3 Piecewise Linear Recursive Convolution Method

Luebbers et al. formulated the first frequency dispersive FDTD algorithm using the recursive convolution (RC) scheme. Later it became piecewise linear recursive convolution (PLRC) method [37]. Initially developed for Debye media [38], the approach was later extended for the study of wave propagation in a Drude material [39], N-th order dispersive media [40], an anisotropic magneto-active plasma [41], ferrite material [42] and the bi-isotropic/chiral media [43, 44, 45] The RC approach, typically being faster and having required fewer computer memory resources than other approaches, is usually less accurate. But in case of multiple pole mediums, it is easier to follow the RC approach.

In the initial derivation of PLRC method for a linear dispersive medium, the relation between electric flux density and electric field intensity is expressed as:

$$D(t) = \varepsilon_\infty\varepsilon_0 E(t) + \varepsilon_0 \int_0^t E(t - \tau)\chi(\tau)d\tau \tag{4.33}$$

Which can be discretized as:

$$D^n = \varepsilon_\infty \varepsilon_0 E^n + \varepsilon_0 \int_0^{n\Delta t} E(n\Delta t - \tau)\chi(\tau)d\tau \tag{4.34}$$

The PRC method is further preceded from this basing discrete equation.

4.4 The General Algorithm

The derivation of equations for multi-pole dispersion relation is more difficult compared to the single pole-pair dispersion relation. For example, for six-pole Lorentz-Drude dispersion the required derivation process is lengthy. Additionally, the memory required for computation is also vast. There are various methods proposed by researchers regarding this topic such as Tafloves matrix inversion method, Multi-term dispersion by Okoniewski, etc. However Alsunaidi and Al-Jabr proposed a general algorithm technique which solves various problems regarding previous methods. The major advantage of this technique is that it requires only one algorithm for any dispersion relation. The dispersive relation has the general form as

$$D(\omega) = \varepsilon(\omega)E(\omega) \tag{4.35}$$

Which can be expressed in terms of summation of poles

$$D(\omega) = \varepsilon_\infty \varepsilon_0 E(\omega) + \sum\nolimits_i^N P_i(\omega) \tag{4.36}$$

Where N is the number of poles. Applying Fourier transform, this equation becomes

$$D^{n+1} = \varepsilon_\infty \varepsilon_0 E^{n+1} + \sum\nolimits_i^N P_i^{n+1} \tag{4.37}$$

or,

$$E^{n+1} = \frac{D^{n+1} - \sum_i^N P_i^{n+1}}{\varepsilon_\infty \varepsilon_0} \tag{4.38}$$

This term P_i can be any form of dispersion relation such as the Debye, the Drude or just the conductivity term. This the final solved equation for E.

5. THEORY OF RING RESONATORS

5.1 Overview

Ring Resonators play an important role in the success of the silicon photonics [46], because silicon allows enables ring resonators of an unprecedented small size. Constructing ring resonators by means of Metal-Insulator-Metal (MIM) alignment have unlocked the potential possibilities of achieving practical attributes. The field of plasmonic ring resonators is very much alive and better understanding a technological advances will definitely give many exciting results in the coming decade both in new physics and in valuable purposes.

5.2 Theoretical Approach

A generic ring resonator consists of an optical waveguide which is looped back on itself such that a resonance occurs when the optical path length of the resonator is exactly a whole number of wavelengths. Ring resonator therefore support multiple resonances and the spacing between these resonances, the free spectral range (FSR), depends on the resonator length. A ring resonator is a unique device if and only if a coupling is done to the outer world. The co-directional coupling mechanism is the custom of coupling used to couple a resonator and adjacent waveguides.

A crude representation of ring resonator is depicted in Figure 5.1 which shows the unidirectional coupling between the resonator and waveguide [47, 35]. Ei1 being the excitation signal, various losses accumulated along the propagation of light can be related by a matrix relationship with attenuation

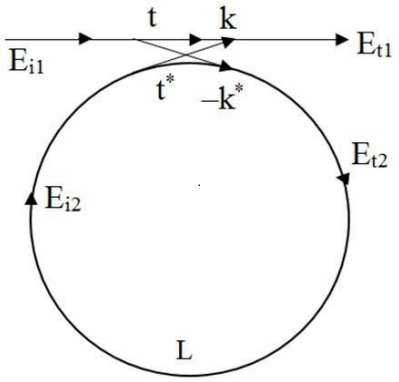

Fig. 5.1: Pivotal Ring Resonator Structure

constants:

$$\begin{pmatrix} E_{t1} \\ E_{t2} \end{pmatrix} = \begin{pmatrix} t & k \\ -k^* & t^* \end{pmatrix} \begin{pmatrix} E_{i1} \\ E_{i2} \end{pmatrix} \tag{5.1}$$

Coupler parameters are described using t and k which depend on coupler mechanism, E_{t1} and E_{t2} denote normalized complex amplitudes. Therefore,

$$|t^2| + |t^2| = 1 \tag{5.2}$$

The transmitted field can be expressed as:

$$E_{t1} = \frac{|t| - Le^{-j(\phi-\phi_t)}1 - |t|Le^{-j(\phi-\phi_t)}}{E}_{i1} e^{\phi t} \tag{5.3}$$

5.3 Applications

Constructing ring resonators using Metal-Insulator-Metal (MIM) alignment have unlocked the potential possibilities of achieving practical attributes such that optical switch [48, 49], directional couplers [50, 51], sensing applications [52, 7, 53] in addition to modulator [54, 55, 56], laser [57] or resonant detectors [58].

6. RING RESONATOR WITH DIVERSE GEOMETRIC CONFIGURAION

6.1 Overview

In this section, simulation results of eight waveguide resonators with rectangular, circular, hexagonal, elliptical geometry as well as special type of rectangles such was diamond and tapered edge shaped were investigated. The numeric analysis was executed by means of Finite Difference Time Domain (FDTD) method. The dimensions of the resonators were considered in the nanometer scale. The results provided an understanding of transmission efficacy of the resonators and will aid the selection process of pertinent design in the insinuated region. Behavioral analysis of the resonators according to their geometric properties will assist to select the design according to applications of interest which were revealed beforehand. The study done in the biological window of wavelength will provide the suitable geometric configuration to use in biological applications.

6.2 Structures and Simulation

6.2.1 Proposed Structures

Figure 6.1 shows the circular structure. The absolute edifice is quantified 1000nm*1000nm. The gray area indicates silver and the white area signifies air. The thickness of the waveguide W=50nm, matched with the breadth of the ring. The coupling gap has been kept at 10nm. The radius of the inner

circle is R=150nm.

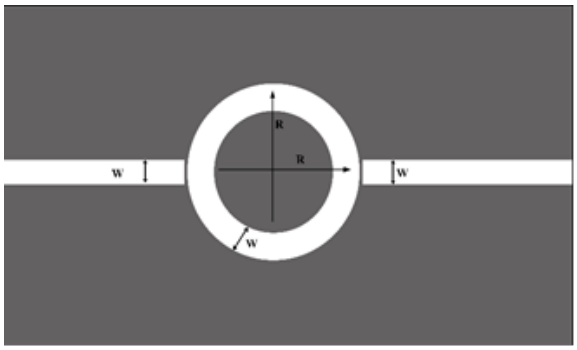

Fig. 6.1: Schematic diagram of circular ring resonator

Figure 6.2 indicates the rectangular resonator, A and B being the length and width. Two resonators were studied with where one of them is constituted with A=400nm and B=275nm and in case of the other one the dimensions were A=400nm and B=550nm. Figure 6.3 represents the angled hexagonal resonator, each side measuring 200nm and the breadth is 50nm for all the resonators. The flat version of the hexagonal resonator was also analyzed. In figure 6.4, the elliptical resonator was depicted. The shape other than the ones in the figures which were considered are a tapered edge square (390nm*390nm) and a diamond (288 nm* 288nm with diagonal=400nm).

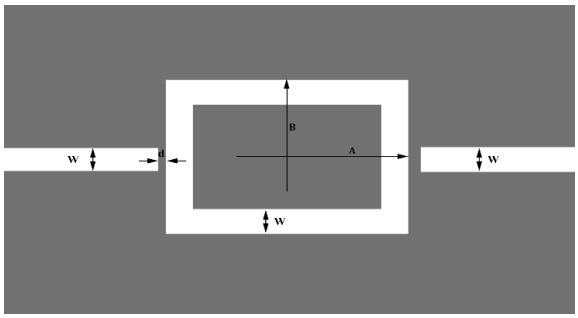

Fig. 6.2: Schematic diagram of rectangular ring resonator

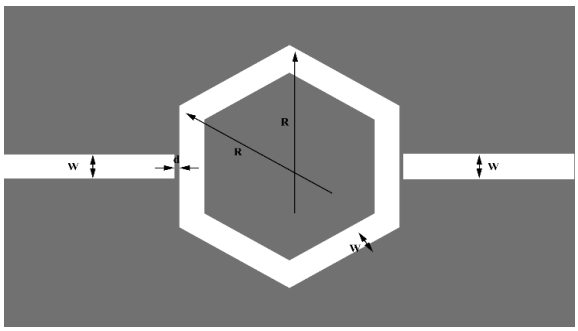

Fig. 6.3: Schematic diagram of hexagonal ring resonator

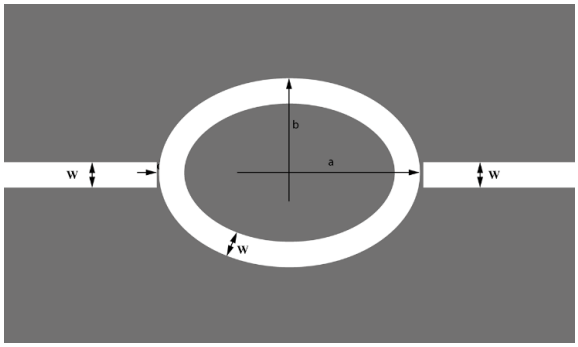

Fig. 6.4: Schematic diagram of elliptical ring resonator

6.2.2 Simulation of Plasmonic Waves

A 2D simulator was programmed using MATLAB [59] to carry out the FDTD operation. The frequency reliant dispersion was patterned using a broad polarization algorithm. Propagation of surface plasmon wave in different resonators are depicted below:

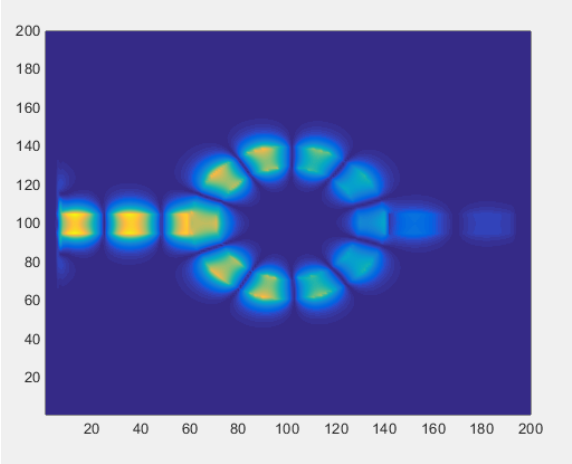

Fig. 6.5: Propagation of surface plasmon wave in circular ring resonator

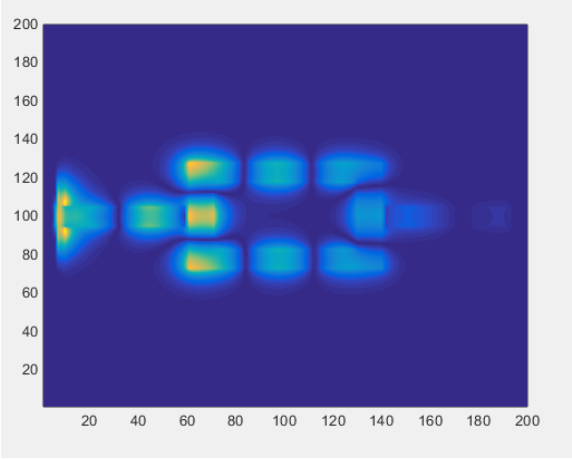

Fig. 6.6: Propagation of surface plasmon wave in rectangular ring resonator

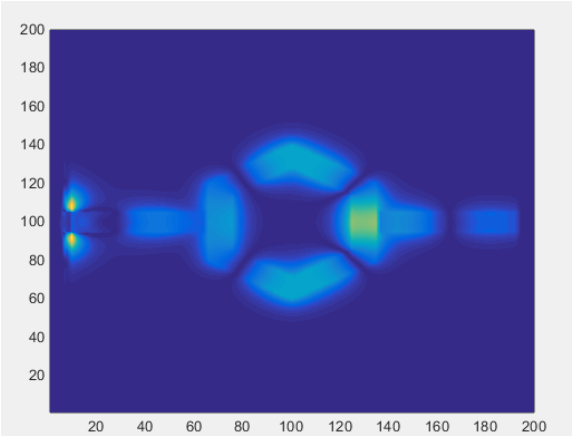

Fig. 6.7: Propagation of surface plasmon wave in hexagonal ring resonator

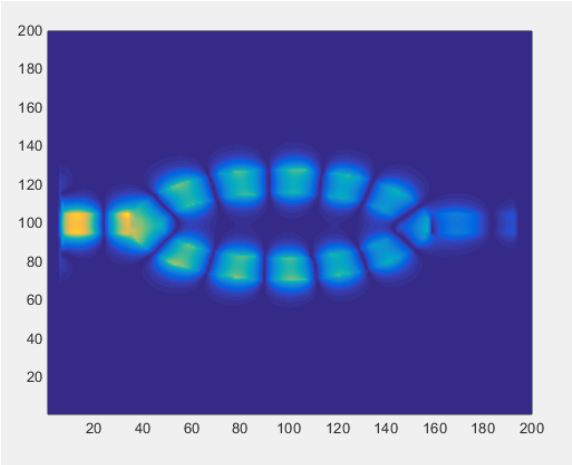

Fig. 6.8: Propagation of surface plasmon wave in elliptical ring resonator

6.3 Result Analysis

6.3.1 Overview

The performance of the resonators were judged by means of transmission efficiency. The percentage of power being received in the output port in the wavelength range of 700nm to 2600nm were calculated using the Poynting vector [60]. The frequency for which the resonator transmits maximum power (resonant frequency) and the modes of propagation was also be enumerated through the analysis.

6.3.2 Transmission Efficiency Analysis

Figure 6.9 to Figure 6.14 have been utilized to depict the overall transmission efficacy of eight resonators in the wavelength region under consideration (700nm to 2600nm) and the rectangles and hexagons have been plotted collectively.

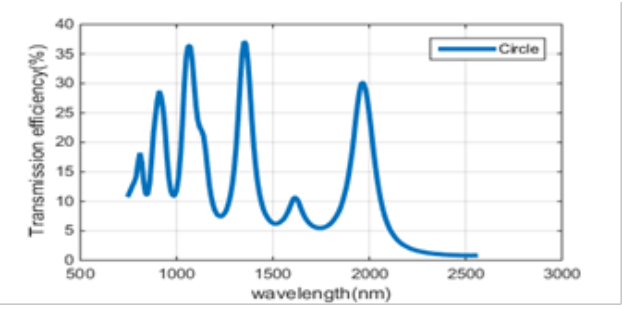

Fig. 6.9: Circular Ring Resonator

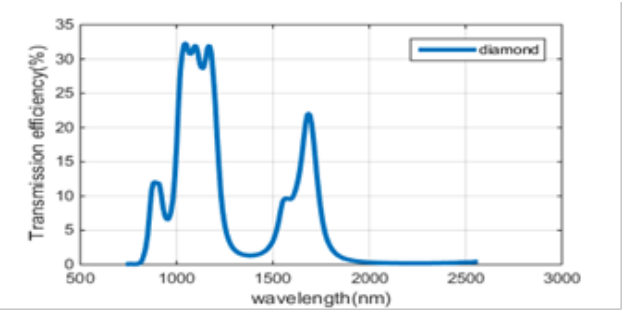

Fig. 6.10: Diamond Shaped Ring Resonator

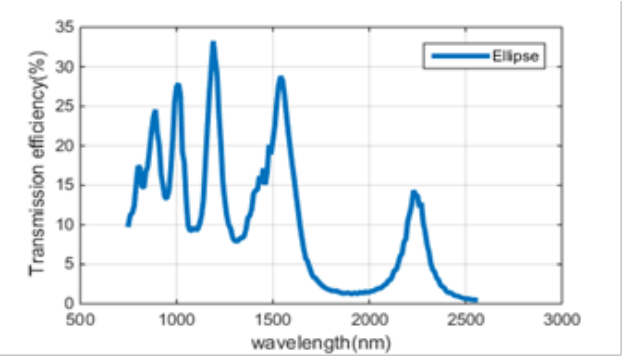

Fig. 6.11: Elliptical Ring Resonator

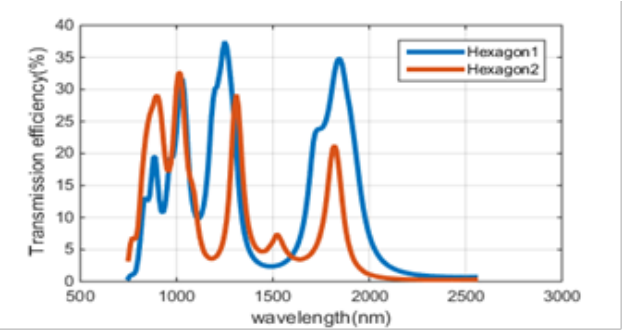

Fig. 6.12: Hexagonal Ring Resonator

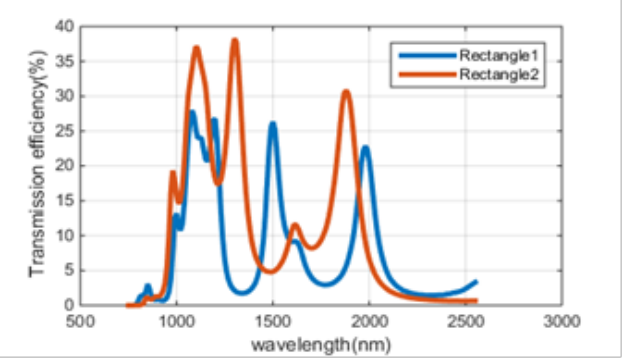

Fig. 6.13: Rectangular Ring Resonator

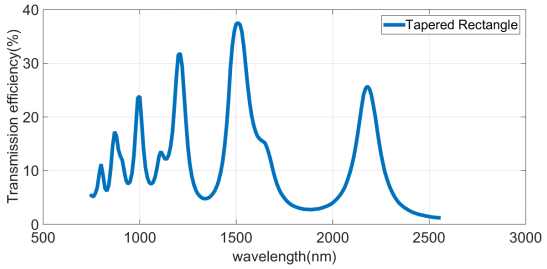

Fig. 6.14: Tapered Edge Ring Resonator

6.3.3 Resonant Frequency Analysis

The resonant frequency within the specified wavelength range for eight resonators were calculated by means of FDTD simulator by iterating each frequency 20000 times. The results are depicted in the subsequent table:

Tab. 6.1: Maximum efficiency analysis

Geometric Structure	**Maximum Efficiency** (%)	**Wavelength**
Circular	37.12	1310nm
Rectangle1(B>A)	27.97	1040nm
Rectangle2(A>B)	38.27	1260nm
Tapered Edge	37.52	1510nm
Diamond	32.23	1000nm
Angled Hexagon	37.47	1210nm
Flat Hexagon	29.21	1270nm
Ellipse	33.25	1150nm

The maximum efficiency (38.27%) is observed for the rectangular ring resonator with dimensions 400nm*275nm in 1260nm wavelength. The resonator with tapered edge rectangle shape also indicated prominent result (37.52%) due to the lower truncation error at the edges. Dependence of maximum efficiency and resonant wavelength on the device geometry is clearly evident from the data.

6.3.4 Electromagnetic Mode Analysis

The resonated state of the resonators is depicted in Figure 6.15 which consists of the linearly polarized mode 9, 7, 5 of the resonators. The N number of nodes in the magnetic field distribution within the resonator refers to mode (N-1) [61]

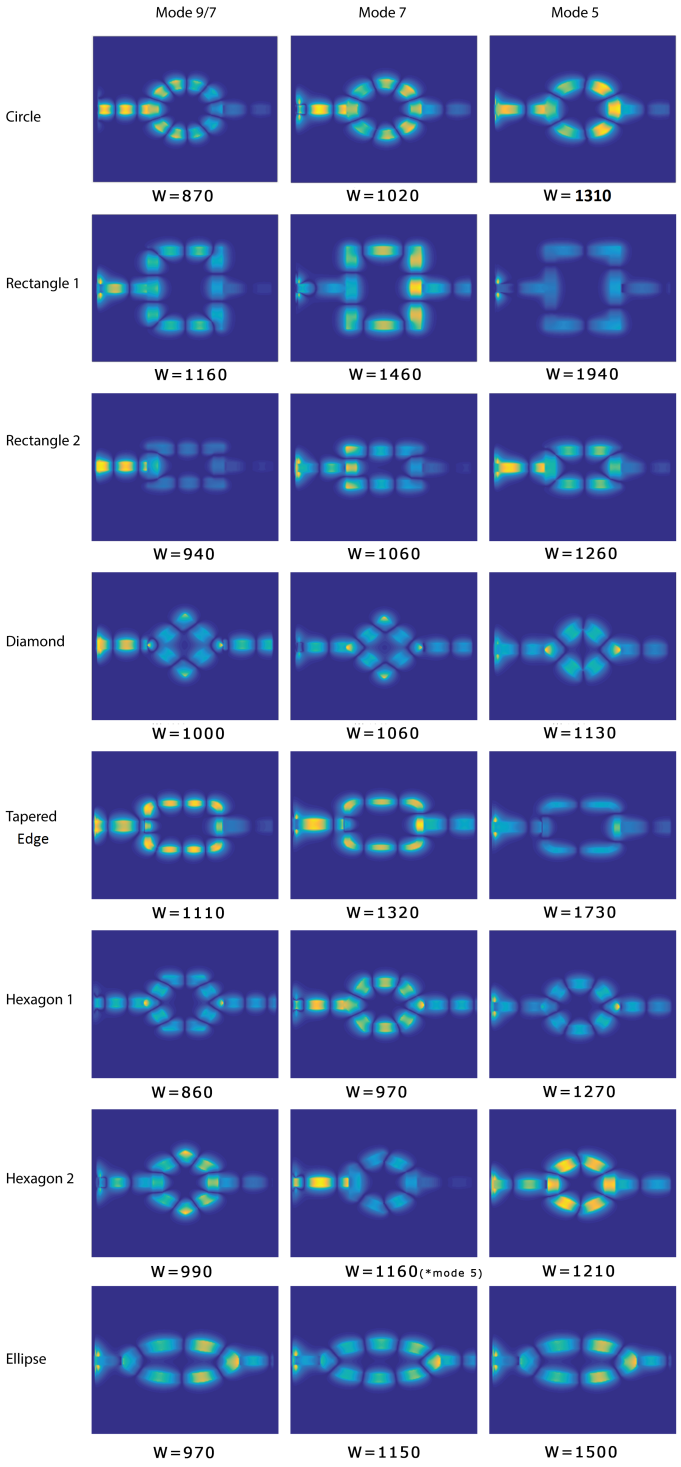

Fig. 6.15: The normalized Hz field distribution of shapes at mode 9, 7, 5 and resonant wavelength. The mode fluctuates with the wavelength of operation.

6.3.5 Performance in Biological Window

990nm to 1100nm wavelength is referred to as the biological window [62, 63] of operation. The transmission properties of the resonators under discussion in this region is presented in Table 6.2.

Tab. 6.2: Performance analysis in biological window

Geometrical Configuration	**Efficiency (%)**	**Biological window**
Circular	36.33	1020nm
Rectangle1(B>A)	27.97	1040nm
Rectangle2(A>B)	37.14	1060nm
Tapered Edge	23.86	1000nm
Diamond	25.36	1110nm
Angled Hexagon	31.67	990nm
Flat Hexagon	15.29	1040nm
Ellipse	33.25	1150nm

Rectangle with dimension 400nm*275nm is the apt configuration to use in the biological window with a transmission efficiency of 37.14% in resonant wavelength of 1060nm. If the design constraints force a designer to use other structures, the resonant wavelengths of alternative structures are also mentioned in Table 6.2, through which one can find the wavelength for which the resonator will be most effective.

7. PERFORMANCE ANALYSIS BY ALTERING DESIGN PARAMETERS

7.1 Overview

In this section, the design parameters of rectangular and elliptical ring resonators were altered and the analysis focused on pinpointing an optimum structure within the specified geometric configurations.

7.2 Rectangular Configuraion

In this section, simulation results of fifteen waveguide resonators with rectangular geometry were investigated. Numeric analysis was executed by means of Finite Difference Time Domain (FDTD) method. A range of dimensions (length*width) was considered in nanometer scale. The results provided an understanding of transmission efficacy of the resonators and will aid the selection process of pertinent design in the insinuated region. Behavioral analysis of the resonators according to their geometric properties will assist to select the applications of interest which were revealed beforehand.

7.2.1 Proposed Desings

One of the proposed rectangular structures has been featured in Figure 7.1. The absolute edifice is quantified 1000nm*1000nm. A and B being the length and width of the resonator, the gray and white color indicates silver and

air respectively. Thickness of the waveguide W=50nm, matched with the breadth of the ring. The coupling gap has been kept at 5nm.

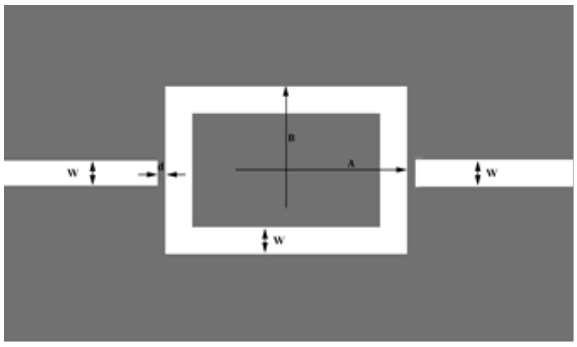

Fig. 7.1: Proposed Rectangular Resonator

Thorough investigation of the effect of altering geometric dimension on transmission properties took place in this paper. Eleven structures were primarily proposed, arbitrarily starting from A and B both being 60nm. A being fixed at 60nm, B was increased with 10nm increment till 100nm. In the second phase, B was kept constant at 60nm and A was increased till 120nm with the unchanged increment. Four more resonators with dimensions 60nm*86nm, 74nm*60nm, 86nm*60nm and 94nm*60nm were simulated to authenticate the outcomes of aforementioned configurations.

7.2.2 Simulation of Resonators

Figure 7.2 includes the resonated state of fifteen structures. By means of Poynting vector [19], power calculation of two ports was accomplished. The performance of the resonators were judged by means of transmission efficiency. The wavelength range was taken from 700nm to 2600nm and FDTD method was iterated for 20000 time steps for each wavelength.

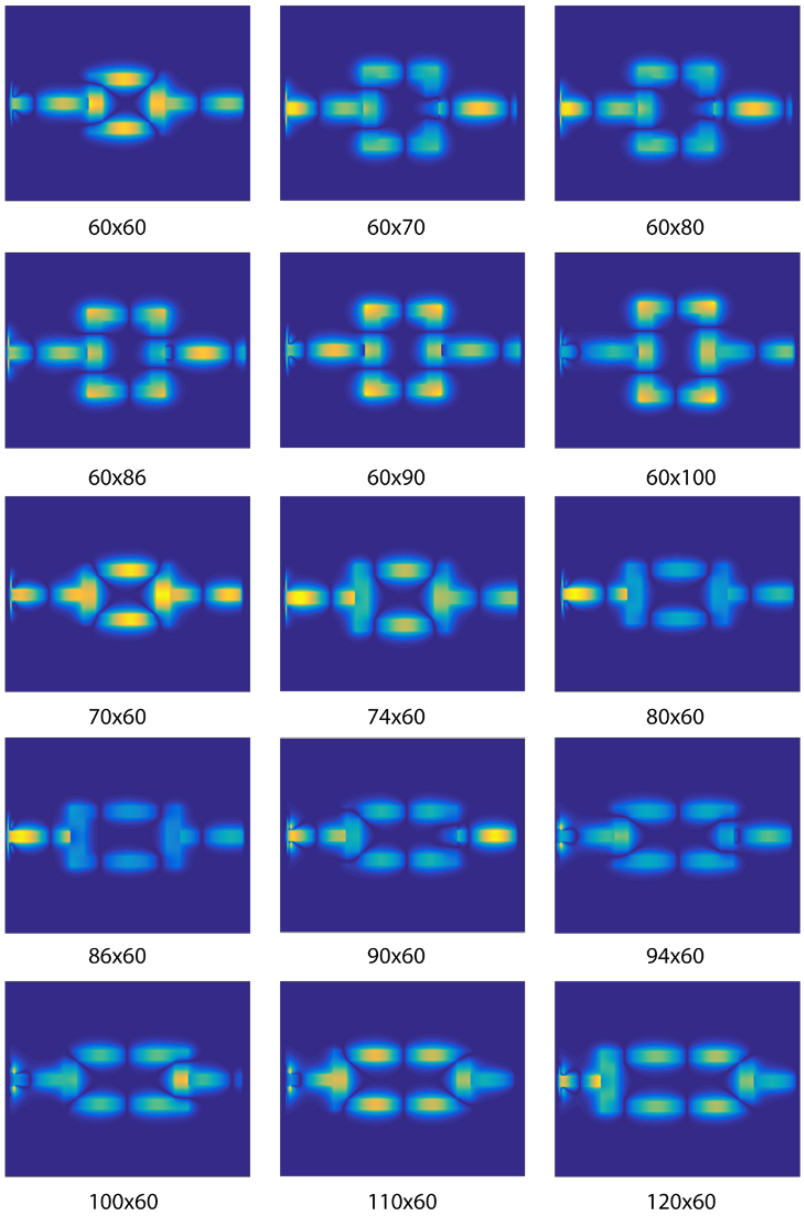

Fig. 7.2: Resonated state of the proposed structures

7.2.3 Result Analysis

Table 7.1 incorporated the values of transmission efficiency along with corresponding dimensions. A graphical illustration which includes Transmission Efficiency vs. Aspect Ratio (B/A) has been exhibited in Figure 7.3.

Tab. 7.1: Dimension of the resonators and their corresponding Transmission Efficiency (%)

Parameter A*B (nm2)	**Aspect Ratio (B/A)**	**Transmission Efficiency (%)**
120*60	0.5000	53.101
110*60	0.5454	53.614
100*60	0.6000	53.928
94*60	0.6382	55.839
90*60	0.6667	56.571
84*60	0.6977	55.894
80*60	0.7500	54.575
74*60	0.8108	54.642
70*60	0.8571	55.752
60*60	1.0000	55.918
60*70	1.1667	56.099
60*80	1.3333	53.546
60*90	1.5000	50.033
60*100	1.6667	48.135

The highest transmission efficiency observed is 56.571% and corresponding dimension is 90nm*60nm. Increase in length (A) further reduces the efficacy. Then again, if B is enlarged, degradation in efficiency occurs yet again. One strident decline was discerned with each increment after 60nm*70nm. Three continuative structures with dimensions 70nm*60nm, 60nm*60nm, 60nm*70nm indicates transmission efficiencies of 55.7518%, 55.9185%, 56.0994% respectively, showing less amount of instability compared to other successive structures, validating the fact that minuscule change in dimension will not immensely affect the transmission properties.

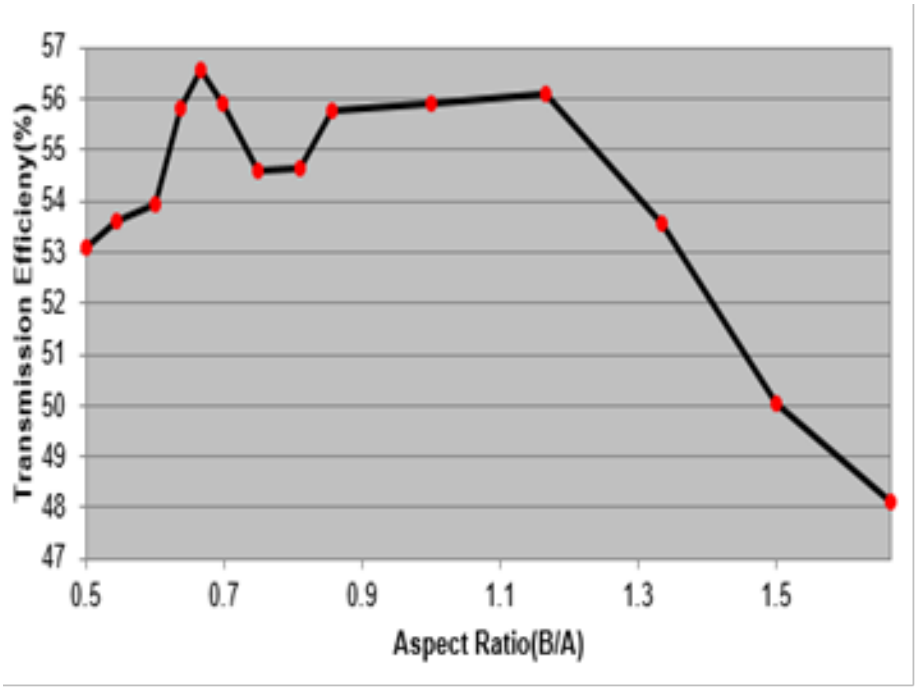

Fig. 7.3: Transmission Efficiency vs. Aspect Ratio of the Resonators

7.3 Elliptical Configuraion

In this section, simulation results of seven waveguide resonators with elliptical geometry were investigated. Numeric analysis was executed by means of Finite Difference Time Domain (FDTD) method. A range of eccentricity was considered. The results provided an understanding of transmission efficacy of the resonators according to the eccentricity of the ellipses.

7.3.1 Proposed Design

One of the proposed elliptical structures has been featured in Figure 7.4. The absolute edifice is quantified 1000nm*1000nm. a and b being the major and minor axis of the resonator, the gray and white color indicates silver and air respectively. Thickness of the waveguide W=50nm, matched with the breadth of the ring. The coupling gap has been kept at 5nm.

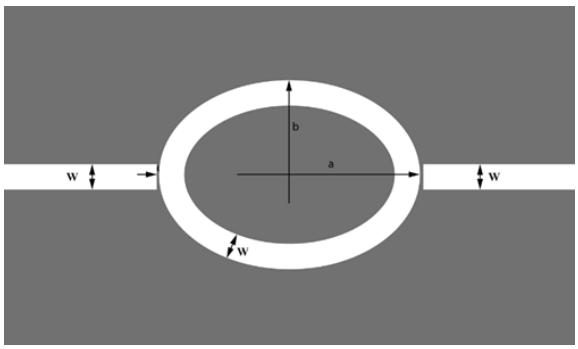

Fig. 7.4: Schematic diagram of elliptical ring resonator

The sequence of the proposed designs were illustrated in figure 7.5 according to the eccentricity of the elliptical resonators. Eccentricity from 0 to 0.75 were depicted by altering the major and minor axes.

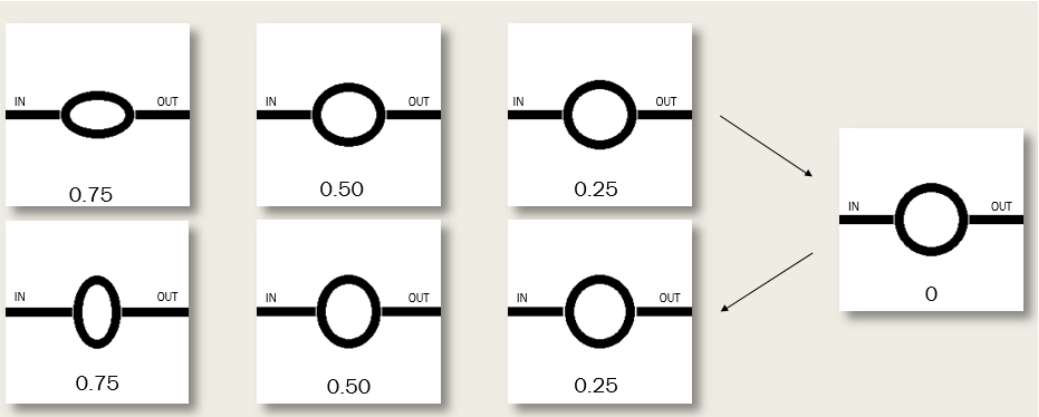

Fig. 7.5: Proposed elliptical ring resonators

7.3.2 Simulation of Resonators

Figure 7.6 indicates the resonated state of an elliptical structure. By means of Poynting vector [19], power calculation of two ports was accomplished. The performance of the resonators were judged by means of transmission efficiency. The wavelength range was taken from 700nm to 2600nm and FDTD method was iterated for 20000 time steps for each wavelength.

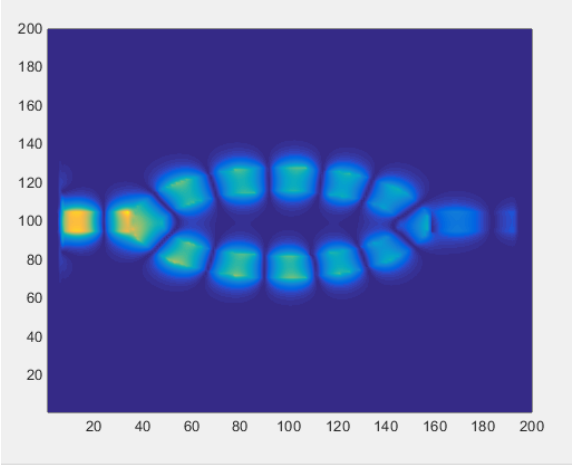

Fig. 7.6: Resonated state of an elliptical ring resonator

7.3.3 Result Analysis

Table 7.2 incorporated the values of transmission efficiency along with corresponding dimensions. A graphical illustration which includes Transmission Efficiency vs. Eccentricity has been exhibited in Figure 7.7

The highest transmission efficiency observed is 58.48% and corresponding dimension eccentricity is 0.75. Efficacy declines as moved forward and from eccentricity -0.50 (negative eccentricity indicates inverted major and minor axis from the positive ones), the efficiency begins to rise once more. Unlike rectangular resonators, an optimum shape is yet to be established.

Tab. 7.2: Eccentricity of the resonators and their corresponding Transmission Efficiency (%)

Parameter(eccentricity)	Maximum Efficiency (%)	Wavelength(nm)
0.75	58.48	1680
0.50	54.90	1310
0.25	54.64	1340
0.00	54.60	1380
-0.25	54.48	1350
-0.50	54.49	1910
-0.75	54.90	1700

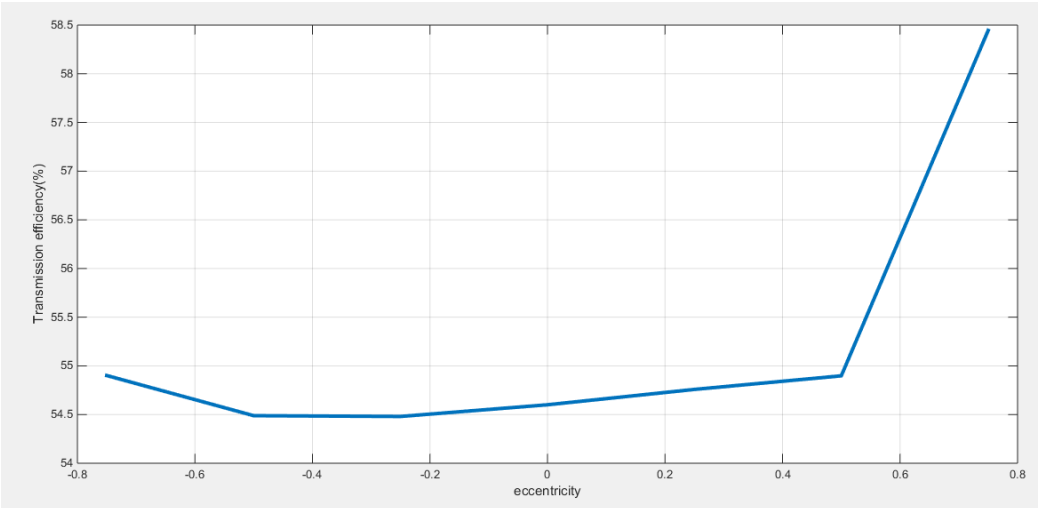

Fig. 7.7: Transmission Efficiency vs. Eccentricity of the Resonators

8. RAT RACE COUPLER

8.1 Overview

A directional coupler is an electronic component having four-port circuits with one port being isolated from the input port and another being considered as a through port. The device is normally used to split the input signal and distributed power. Example - Rat race coupler, Tee coupler.

Rat-race coupler (RRC) is a 3dB coupler which consists of four transmission lines with impedance of $\sqrt{2Z_0}$, three with length of $\lambda/4$ and one with length of $3\lambda/4$. There are four terminals with impedance of Z_0 [64]

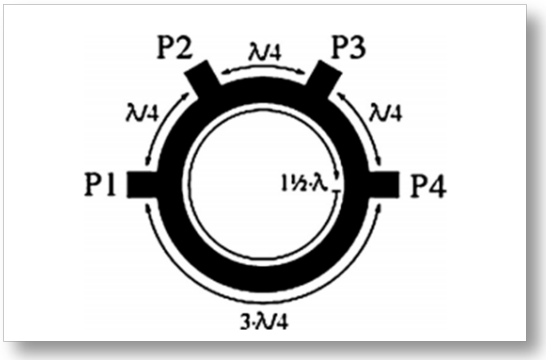

Fig. 8.1: Schematic diagram of a rat race coupler

A normal three-port Tee junction is taken and a fourth port is added to it, to make it a rat race junction. All of these ports are connected in angular ring forms at equal intervals using series or parallel junctions. The preceding Figure 8.1 shows a novel rat race coupler.

8.2 Structure and Design

Plasmonic Rat Race couplers of nanometer scale and micrometer scale have been proposed and investigated. The absolute area is reckoned 1000nm*1000nm. Radius of the rat race junction have been taken 200nm, 250nm and 300nm. The gray and white color indicates silver and air respectively. Thickness of the waveguide is 50nm, matched with the breadth of the coupler. No coupling gap has been kept. Proposed structures are depicted below in Figure 8.2-Figure 8.4:

Fig. 8.2: RRC with 200nm radius, λ=838nm

Fig. 8.3: RRC with 250nm radius, λ=1047nm

Fig. 8.4: RRC with 300nm radius, λ=1257nm

8.3 MATLAB Simulation

8.3.1 Simulation

Figure 8.5 includes the resonated state of a coupler. By means of Poynting vector, power calculation of two ports was accomplished. The performance of the couplers were judged by means of transmission efficiency. The wavelengths were taken 838nm, 1047nm, 1257nm for 200nm, 250nm and 300nm radius couplers respectively. FDTD method was iterated for 20000 time steps for each wavelength.

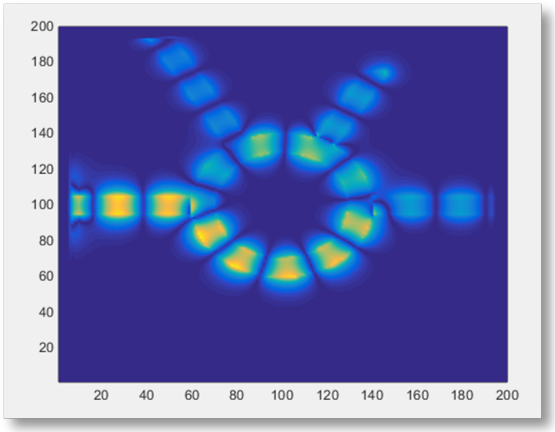

Fig. 8.5: Resonated state of an RRC with radius of 250nm

8.3.2 Results Analysis

The transmission of power in the RRC with 200nm radius is 1.05% through port 2, 6.772% through port 3 and 7.7168% through port 4. Similarly for 250nm radius, 1.6821% through port 2, 3.59% through port 3 and 20.25% through port 4 and for 300nm radius, 2.55% through port 2, 3.06% through port 3 and 25.93% through port 4. The bar plot of the power transmitted through the ports are depicted in the following Figure 8.6, 8.7 and 8.8.

The results found from this analysis so far does not conform to the theory. Therefore, suitable parameters for designing nanometer scale plasmonic rat race coupler are yet to be discovered.

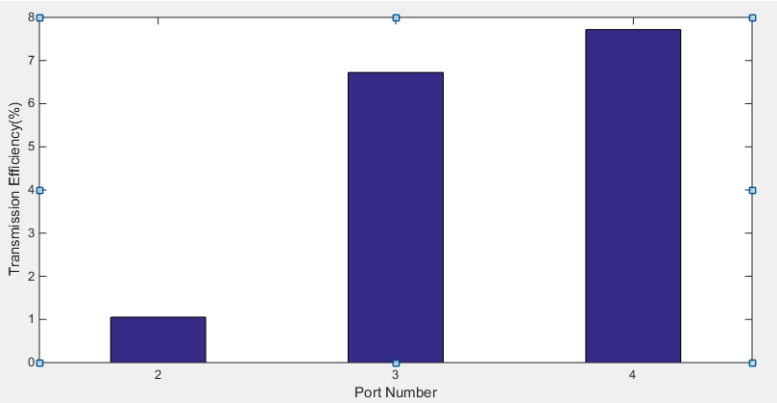

Fig. 8.6: Efficiency of ports of an RRC with a radius of 200nm

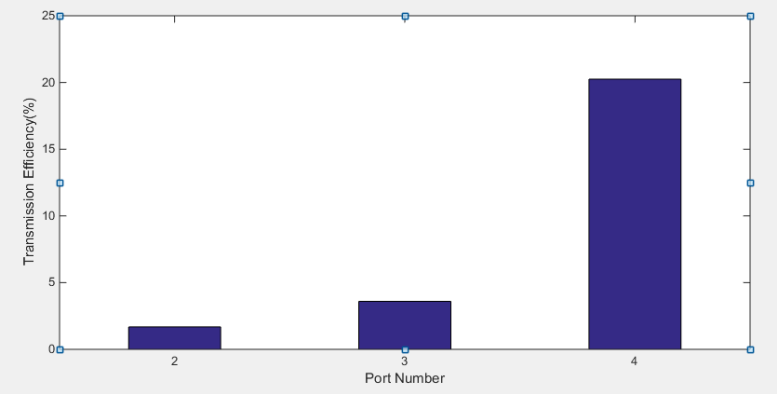

Fig. 8.7: Efficiency of ports of an RRC with a radius of 250nm

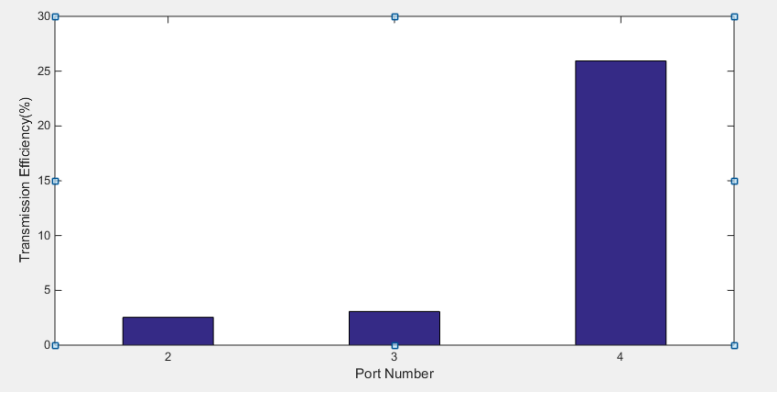

Fig. 8.8: Efficiency of ports of an RRC with a radius of 300nm

8.4 CST Simulation

To investigate the S-parameters of the rat race coupler, micrometer scale couplers were designed and simulated in CST. Frequency domain solver was utilized and the numeric approach was Finite Element Method (FEM). The radius of the coupler was taken as 3.5m along with a 0.5m thickness. A frequency sweep from 150 THz to 250 THz was used for this operation. The device material was Silicon and substrate materials were Silicon Dioxide and Silicon Nitride respectively.

8.4.1 Silicon Dioxide Substrate

Figure 8.9 shows the RRC with device material silicon over a substrate of Silicon Dioxide. The resulting S-parameters of four ports are plotted in the following figure 8.10. The declination from theory is evident through the

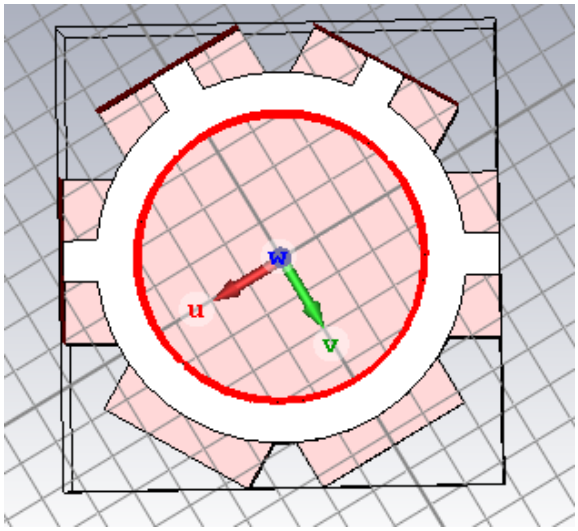

Fig. 8.9: RRC with Silicon Dioxide substrate

results. The substrate was changed to observe the alteration of results.

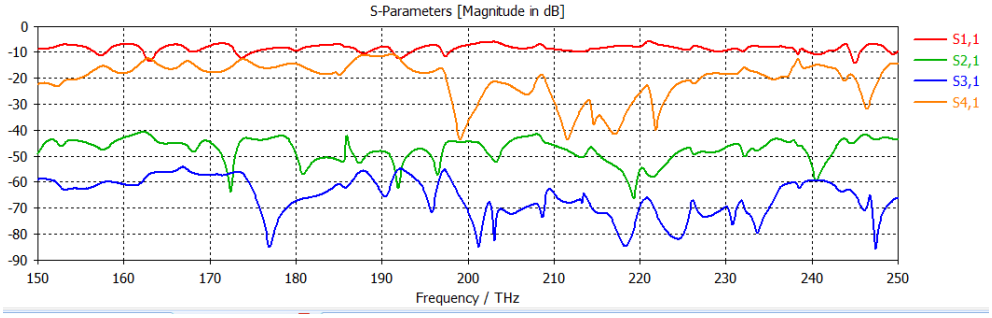

Fig. 8.10: S-Parameters of RRC with Silicon Dioxide substrate

8.4.2 Silicon Nitride Substrate

Figure 8.11 shows the RRC with device material silicon over a substrate of Silicon Dioxide. The resulting S-parameters of four ports are plotted in the following Figure 8.12.

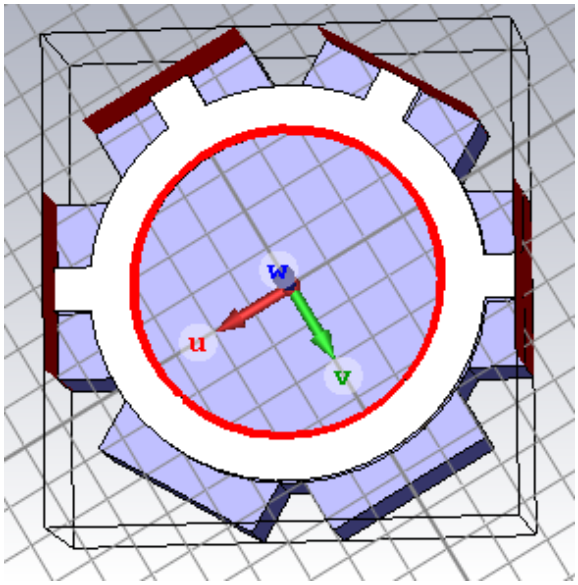

Fig. 8.11: RRC with Silicon Dioxide substrate

No significant improvement has been observed by changing the substrate material to Silicon Nitride. Alternative approaches to solve the predicament are being investigated.

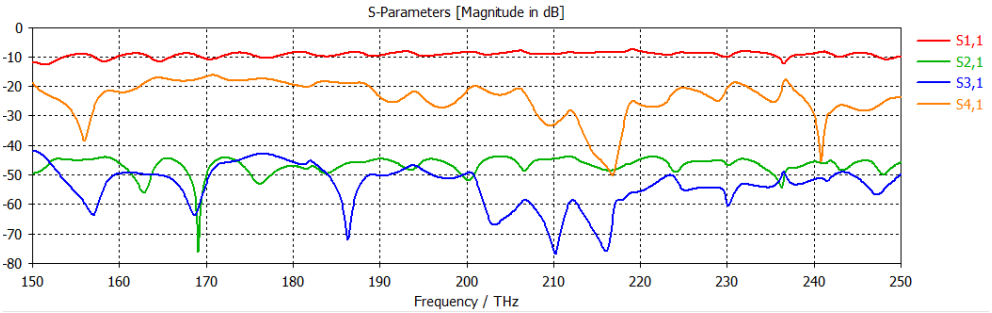

Fig. 8.12: S-Parameters of RRC with Silicon Dioxide substrate

9. CONCLUSION AND FUTURE PLANS

9.1 Conclusion

In recent years, plasmonic components have rapidly evolved from discrete, passive structures toward integrated active devices that could comprise an all optical, nano photonic networking technology. In this paper, theoretical approach of implementing plasmonic nanostructures and comprehensive analysis of transmission properties took place. The accomplished tasks at a glance are as followed:

- Design and simulation of ring resonators by altering geometric configuration of the ring resonators.
- Investigating performance of rectangular ring resonators by varying design parameters.
- Investigating performance of elliptical ring resonators by altering eccentricity of the resonator.
- Designing nanoscale plasmonic rat race couplers and investigating transmission efficiency and S-Parameters of the ports.

9.2 Future Plans

The nanostructures which were proposed and simulated showed great potential but more research is due, to achieve novel designs. Implementing of the devices in future is of topmost priority. Following are the clearer view of what schemes lie ahead for upcoming days:

- Testing the devices in pragmatic applications such as filter, mixer, sensor etc.
- Achieving novel designs of the proposed structures.
- Finding the optimum design parameters for elliptical ring resonators.
- Achieving anticipated performance in plasmonic rat race coupler.
- Designing universal logic gates i.e. NAND and NOR gates.
- Designing logic circuits e.g. multiplexers, demultiplexers, encoders etc.
- Real life implementation of the proposed structures and investigating their results with the simulation ones.

BIBLIOGRAPHY

[1] W. L. Barnes, A. Dereux, and T. W. Ebbesen, "Surface plasmon subwavelength optics," *Nature*, vol. 424, no. 6950, pp. 824–830, 2003.

[2] S. A. Maier, *Plasmonics: fundamentals and applications*. Springer Science & Business Media, 2007.

[3] D. K. Gramotnev and S. I. Bozhevolnyi, "Plasmonics beyond the diffraction limit," *Nature photonics*, vol. 4, no. 2, pp. 83–91, 2010.

[4] R. J. Blaikie and D. O. Melville, "Imaging through planar silver lenses in the optical near field," *Journal of Optics A: Pure and Applied Optics*, vol. 7, no. 2, p. S176, 2005.

[5] D. O. Melville and R. J. Blaikie, "Super-resolution imaging through a planar silver layer," *Optics express*, vol. 13, no. 6, pp. 2127–2134, 2005.

[6] A. Hosseini and Y. Massoud, "A low-loss metal-insulator-metal plasmonic bragg reflector," *Optics express*, vol. 14, no. 23, pp. 11318–11323, 2006.

[7] A. J. Haes and R. P. Van Duyne, "A nanoscale optical biosensor: sensitivity and selectivity of an approach based on the localized surface plasmon resonance spectroscopy of triangular silver nanoparticles," *Journal of the American Chemical Society*, vol. 124, no. 35, pp. 10596–10604, 2002.

[8] J. Henzie, M. H. Lee, and T. W. Odom, "Multiscale patterning of plasmonic metamaterials," *Nature nanotechnology*, vol. 2, no. 9, pp. 549–554, 2007.

[9] V. E. Ferry, L. A. Sweatlock, D. Pacifici, and H. A. Atwater, "Plasmonic nanostructure design for efficient light coupling into solar cells," *Nano letters*, vol. 8, no. 12, pp. 4391–4397, 2008.

[10] S. Y. Chou and W. Ding, "Ultrathin, high-efficiency, broad-band, omni-acceptance, organic solar cells enhanced by plasmonic cavity with sub-wavelength hole array," *Optics express*, vol. 21, no. 101, pp. A60–A76, 2013.

[11] A. Bhadauria and S. Sharma, "Optically controlled reflection type rf phase shifter using rat-race coupler on silicon substrate," in *Devices, Circuits and Systems (ICDCS), 2016 3rd International Conference on*, pp. 319–321, IEEE, 2016.

[12] S. Koziel, A. Bekasiewicz, and P. Kurgan, "Rapid design optimization of miniaturized rat-race coupler using multi-fidelity electromagnetic models," in *Applied Computational Electromagnetics (ACES), 2015 31st International Review of Progress in*, pp. 1–2, IEEE, 2015.

[13] K.-K. M. Cheng and S. Yeung, "A novel rat-race coupler with tunable power dividing ratio, ideal port isolation, and return loss performance," *IEEE Transactions on Microwave Theory and Techniques*, vol. 61, no. 1, pp. 55–60, 2013.

[14] G. Chaudhary and Y. Jeong, "Arbitrary power division ratio rat-race coupler with negative group delay characteristics," *IEEE Microwave and Wireless Components Letters*, vol. 26, no. 8, pp. 565–567, 2016.

[15] C.-L. Kuo, C.-C. Kuo, C.-H. Lien, J.-H. Tsai, and H. Wang, "A novel reduced-size rat-race broadside coupler and its application for cmos distributed sub-harmonic mixer," *IEEE Microwave and Wireless Components Letters*, vol. 18, no. 3, pp. 194–196, 2008.

[16] H. Zhang and K. Chen, "Design of dual-band rat-race couplers," *IET microwaves, antennas & propagation*, vol. 3, no. 3, pp. 514–521, 2009.

[17] Z. Wang, J.-S. Jang, and C.-W. Park, "Tri-band rat-race coupler using resonators," in *Microwave Technology & Computational Electromagnetics (ICMTCE), 2011 IEEE International Conference on*, pp. 186–189, IEEE, 2011.

[18] S. Koziel and A. Bekasiewicz, "Novel structure and size-reduction-oriented design of microstrip compact rat-race coupler," in *Wireless Information Technology and Systems (ICWITS) and Applied Computational Electromagnetics (ACES), 2016 IEEE/ACES International Conference on*, pp. 1–2, IEEE, 2016.

[19] C.-H. Tseng and C.-L. Chang, "A rigorous design methodology for compact planar branch-line and rat-race couplers with asymmetrical t-structures," *IEEE Transactions on Microwave Theory and Techniques*, vol. 60, no. 7, pp. 2085–2092, 2012.

[20] E. Verhagen, *Subwavelength light confinement with surface plasmon polaritons*. PhD thesis, Utrecht University, 2009.

[21] A. Archambault, T. V. Teperik, F. Marquier, and J.-J. Greffet, "Surface plasmon fourier optics," *Physical Review B*, vol. 79, no. 19, p. 195414, 2009.

[22] E. Jin and X. Xu, "Plasmonic effects in near-field optical transmission enhancement through a single bowtie-shaped aperture," *Applied Physics B: Lasers and Optics*, vol. 84, no. 1, pp. 3–9, 2006.

[23] J. T. Krug, E. J. Sánchez, and X. S. Xie, "Design of near-field optical probes with optimal field enhancement by finite difference time domain electromagnetic simulation," *The Journal of chemical physics*, vol. 116, no. 24, pp. 10895–10901, 2002.

[24] R. H. Sagor, K. A. Shahriar, M. G. Saber, and M. R. Amin, "Extraction of modeling parameters for low-loss alternative plasmonic material," *Procedia-Social and Behavioral Sciences*, vol. 195, pp. 2061–2066, 2015.

[25] A. D. Rakić, A. B. Djurišić, J. M. Elazar, and M. L. Majewski, "Optical properties of metallic films for vertical-cavity optoelectronic devices," *Applied optics*, vol. 37, no. 22, pp. 5271–5283, 1998.

[26] M. A. Ordal, R. J. Bell, R. W. Alexander, L. L. Long, and M. R. Querry, "Optical properties of fourteen metals in the infrared and far infrared: Al, co, cu, au, fe, pb, mo, ni, pd, pt, ag, ti, v, and w.," *Applied optics*, vol. 24, no. 24, pp. 4493–4499, 1985.

[27] G. Veronis and S. Fan, "Bends and splitters in metal-dielectric-metal subwavelength plasmonic waveguides," *Applied physics letters*, vol. 87, no. 13, p. 131102, 2005.

[28] H. Gao, H. Shi, C. Wang, C. Du, X. Luo, Q. Deng, Y. Lv, X. Lin, and H. Yao, "Surface plasmon polariton propagation and combination in y-shaped metallic channels," *Optics express*, vol. 13, no. 26, pp. 10795–10800, 2005.

[29] B. Wang and G. P. Wang, "Surface plasmon polariton propagation in nanoscale metal gap waveguides," *Optics letters*, vol. 29, no. 17, pp. 1992–1994, 2004.

[30] G. Veronis and S. Fan, "Theoretical investigation of compact couplers between dielectric slab waveguides and two-dimensional metal-dielectric-metal plasmonic waveguides," *Optics Express*, vol. 15, no. 3, pp. 1211–1221, 2007.

[31] P. Ginzburg and M. Orenstein, "Plasmonic transmission lines: from micro to nano scale with $\lambda/4$ impedance matching," *Optics express*, vol. 15, no. 11, pp. 6762–6767, 2007.

[32] D. Pile and D. K. Gramotnev, "Adiabatic and nonadiabatic nanofocusing of plasmons by tapered gap plasmon waveguides," *Applied Physics Letters*, vol. 89, no. 4, p. 041111, 2006.

[33] R. Wahsheh, Z. Lu, and M. Abushagur, "Nanoplasmonic air-slot coupler: design and fabrication," in *Frontiers in optics*, pp. FTh4A–6, Optical Society of America, 2012.

[34] B. Liu, Y.-F. Liu, S.-J. Li, and X.-D. He, "Rotation and conversion of transmission mode based on a rotatable elliptical core ring resonator," *Optics Communications*, vol. 369, pp. 44–49, 2016.

[35] S. Robinson and R. Nakkeeran, "Photonic crystal ring resonator based bandpass filter," in *Communication Control and Computing Technologies (ICCCCT), 2010 IEEE International Conference on*, pp. 83–85, IEEE, 2010.

[36] H. Saini, "Photonic crystal based rat race coupler for optical applications," *Optik-International Journal for Light and Electron Optics*, vol. 124, no. 17, pp. 3146–3148, 2013.

[37] R. Luebbers, F. P. Hunsberger, K. S. Kunz, R. B. Standler, and M. Schneider, "A frequency-dependent finite-difference time-domain formulation for dispersive materials," *IEEE Transactions on Electromagnetic Compatibility*, vol. 32, no. 3, pp. 222–227, 1990.

[38] F. Hunsberger, R. Luebbers, and K. Kunz, "Finite-difference time-domain analysis of gyrotropic media. i. magnetized plasma," *IEEE Transactions on Antennas and Propagation*, vol. 40, no. 12, pp. 1489–1495, 1992.

[39] D. F. Kelley and R. J. Luebbers, "Piecewise linear recursive convolution for dispersive media using fdtd," *IEEE Transactions on Antennas and Propagation*, vol. 44, no. 6, pp. 792–797, 1996.

[40] J. L. Young, "Propagation in linear dispersive media: Finite difference time-domain methodologies," *IEEE Transactions on Antennas and Propagation*, vol. 43, no. 4, pp. 422–426, 1995.

[41] A. Akyurtlu and D. H. Werner, "Bi-fdtd: A novel finite-difference time-domain formulation for modeling wave propagation in bi-isotropic media," *IEEE Transactions on Antennas and Propagation*, vol. 52, no. 2, pp. 416–425, 2004.

[42] R. J. Luebbers, F. Hunsberger, and K. S. Kunz, "A frequency-dependent finite-difference time-domain formulation for transient propagation in plasma," *IEEE Transactions on Antennas and Propagation*, vol. 39, no. 1, pp. 29–34, 1991.

[43] R. J. Luebbers and F. Hunsberger, "Fdtd for nth-order dispersive media," *IEEE transactions on Antennas and Propagation*, vol. 40, no. 11, pp. 1297–1301, 1992.

[44] A. Grande, I. Barba, A. C. Cabeceira, J. Represa, P. P. So, and W. J. Hoefer, "Fdtd modeling of transient microwave signals in dispersive and lossy bi-isotropic media," *IEEE transactions on microwave theory and techniques*, vol. 52, no. 3, pp. 773–784, 2004.

[45] A. Akyurtlu and D. H. Werner, "A novel dispersive fdtd formulation for modeling transient propagation in chiral metamaterials," *IEEE Transactions on Antennas and Propagation*, vol. 52, no. 9, pp. 2267–2276, 2004.

[46] W. Bogaerts, P. De Heyn, T. Van Vaerenbergh, K. De Vos, S. Kumar Selvaraja, T. Claes, P. Dumon, P. Bienstman, D. Van Thourhout, and R. Baets, "Silicon microring resonators," *Laser & Photonics Reviews*, vol. 6, no. 1, pp. 47–73, 2012.

[47] R. Arefin, M. O. Faruque, R. Al Mahmud, and R. H. Sagor, "Design of a tunable ring resonator with enhanced quality factor," in *Electrical and Computer Engineering (ICECE), 2016 9th International Conference on*, pp. 369–372, IEEE, 2016.

[48] G. Wurtz, R. Pollard, and A. Zayats, "Optical bistability in nonlinear surface-plasmon polaritonic crystals," *Physical review letters*, vol. 97, no. 5, p. 057402, 2006.

[49] H. Lu, X. Liu, L. Wang, Y. Gong, and D. Mao, "Ultrafast all-optical switching in nanoplasmonic waveguide with kerr nonlinear resonator," *Optics express*, vol. 19, no. 4, pp. 2910–2915, 2011.

[50] T. Xu, Y. Zhao, D. Gan, C. Wang, C. Du, and X. Luo, "Directional excitation of surface plasmons with subwavelength slits," *Applied Physics Letters*, vol. 92, no. 10, p. 101501, 2008.

[51] Y. Gong, X. Liu, L. Wang, and Y. Zhang, "Unidirectional manipulation of surface plasmon polariton by dual-nanocavity in a t-shaped waveguide," *Optics Communications*, vol. 284, no. 3, pp. 795–798, 2011.

[52] M. Sumetsky, "Optimization of optical ring resonator devices for sensing applications," *Optics letters*, vol. 32, no. 17, pp. 2577–2579, 2007.

[53] S. Enoch, R. Quidant, and G. Badenes, "Optical sensing based on plasmon coupling in nanoparticle arrays," *Optics express*, vol. 12, no. 15, pp. 3422–3427, 2004.

[54] J. K. Doylend and A. P. Knights, "The evolution of silicon photonics as an enabling technology for optical interconnection," *Laser & Photonics Reviews*, vol. 6, no. 4, pp. 504–525, 2012.

[55] Q. Xu, B. Schmidt, S. Pradhan, and M. Lipson, "Micrometre-scale silicon electro-optic modulator," *nature*, vol. 435, no. 7040, pp. 325–327, 2005.

[56] S. Manipatruni, Q. Xu, B. Schmidt, J. Shakya, and M. Lipson, "High speed carrier injection 18 gb/s silicon micro-ring electro-optic modulator," in *Lasers and Electro-Optics Society, 2007. LEOS 2007. The 20th Annual Meeting of the IEEE*, pp. 537–538, IEEE, 2007.

[57] T. Baba, S. Akiyama, M. Imai, N. Hirayama, H. Takahashi, Y. Noguchi, T. Horikawa, and T. Usuki, "50-gb/s ring-resonator-based silicon modulator," *Optics express*, vol. 21, no. 10, pp. 11869–11876, 2013.

[58] M. T. Hill, H. J. Dorren, T. De Vries, X. J. Leijtens, J. H. Den Besten, B. Smalbrugge, Y.-S. Oei, H. Binsma, G.-D. Khoe, and M. K. Smit, "A fast low-power optical memory based on coupled micro-ring lasers," *nature*, vol. 432, no. 7014, pp. 206–209, 2004.

[59] K. Yee, "Numerical solution of initial boundary value problems involving maxwell's equations in isotropic media," *IEEE Transactions on antennas and propagation*, vol. 14, no. 3, pp. 302–307, 1966.

[60] L. Allen and M. Padgett, "The poynting vector in laguerre–gaussian beams and the interpretation of their angular momentum density," *Optics Communications*, vol. 184, no. 1, pp. 67–71, 2000.

[61] J. Chen, Y. Li, Z. Chen, J. Peng, J. Qian, J. Xu, and Q. Sun, "Tunable resonances in the plasmonic split-ring resonator," *IEEE Photonics Journal*, vol. 6, no. 3, pp. 1–6, 2014.

[62] L. A. Sordillo, Y. Pu, S. Pratavieira, Y. Budansky, and R. R. Alfano, "Deep optical imaging of tissue using the second and third near-infrared spectral windows," *Journal of biomedical optics*, vol. 19, no. 5, pp. 056004–056004, 2014.

[63] M. Golic, K. Walsh, and P. Lawson, "Short-wavelength near-infrared spectra of sucrose, glucose, and fructose with respect to sugar concentration and temperature," *Applied spectroscopy*, vol. 57, no. 2, pp. 139–145, 2003.

[64] E. Stoja and F. Frezza, "Metal-insulator-metal (mim) plasmonic waveguide based directional couplers operating at telecom wavelengths," in *Millimeter Waves and THz Technology Workshop (UCMMT), 2013 6th UK, Europe, China*, pp. 1–2, IEEE, 2013.